The fate of South America's endemic mammalian fauna in response to the most dramatic Cenozoic climate disruption

Lucas Buffan[1,*], Fabien L. Condamine[1], Narla S. Stutz[1], François Pujos[2], Pierre-Olivier Antoine[1]
Laurent Marivaux[1]

[1] Institut des Sciences de l'Evolution de Montpellier, Université de Montpellier, CNRS, IRD, Place Eugène Bataillon, 34095 Montpellier cedex 5, France
[2] IANIGLA, CCT–CONICET–Mendoza, Avenida Ruiz Leal s/n, Parque General San Martín, 5500 Mendoza, Argentina

* **Corresponding author**: Lucas.Buffan@umontpellier.fr

This PDF file includes:

- Extended Materials and Methods
- Manual cleaning details
- Supp. Figures 1 to 41
- Supp. Tables 1 to 9
- SI references

Other supporting materials for this manuscript include the following:

- Raw and cleaned occurrence data (https://doi.org/10.6084/m9.figshare.26495989)

Supplementary text

1. Extended Materials and methods

Fossil data compilation

We first downloaded all Cenozoic mammal occurrences at least with a genus-level resolution from South America from The Paleobiology Database (`?base_name=Mammalia&taxo_reso=genus&cc=SOA`) on 2023-12-11 (n=10,440 occurrences). Because diversification regimes do not occur in the same way on land and in the sea (1), and because the scope of this paper is terrestrial, we removed taxa with marine affinities, *i.e.*, occurrences assigned to the orders "Cetacea" and "Sirenia" or the families "Otariidae" and "Phocidae" (n=354 occurrences). Subsequently, as ref. (2) performed an intensive cleaning of a significant proportion of South American mammalian fossil occurrences (especially Sparassodonts and Native Ungulates), we matched the time ranges of the occurrences we shared with them to those that they proposed (n=2,998 occurrences). For the remaining occurrences, we ensured that their time ranges matched the boundaries of their associated interval. For instance, the Mustersan occurrences were all found to be associated with the 48–42 Ma interval. However, radiochronological evidence has shown that this age is younger, constraining its boundaries to 38.2–35 Ma (conservative estimates have even constrained it to 38.2–38 Ma, based on the only clear datations from well-defined levels) (3) (**Fig. S1**). It is quite concerning to see that such major changes remain uncorrected, especially in public encyclopedies, often used as primary sources of information for non-specialists (*e.g.*, https://en.wikipedia.org/wiki/Mustersan). Age boundaries were expressed as either an International Chronostratigraphic Chart (ICC) stage/epoch or a South American Land Mammal Age (SALMA). In the latter case, we used a SALMA scale built de-novo based on a literature review (*e.g.*, 4). Then, based on the literature and the expertise of the co-authors, we manually revised the entire dataset, occurrence by occurrence. This "manual cleaning" aimed at correcting errors in the database, mostly regarding the age range and the taxonomic assignment (*e.g.*, synonymized genus names, typos, missing elements of open nomenclature) of each occurrence (**Fig. S2**). We intended to make this step as clear as possible by documenting most of the changes we made, and why (*see Manual Occurrence Cleaning part*). Finally, in order to decrease the number of parameters to estimate, we restricted our dataset to the late Paleocene-Early Miocene (60–16 Ma). The final dataset comprised 3,384 occurrences, including 529 genera and 1,108 identified species (see **Tab. S1** for a more detailed description of the data). Occurrence data can be found at https://doi.org/10.6084/m9.figshare.26495989.

Further input treatments

Subsequent data manipulation and visualization were carried out using the Tidyverse (5) suite of R packages, the paleoverse (6) and the deeptime (7) R packages. Out of 3,384 occurrences, 2,108 occurrences (representing *approx.* 62% of the total) were assigned to a SALMA. Due to temporal gaps in the South American Mammal fossil record this timescale is not continuous (**Fig. S1**). Yet, gaps can highly bias fossil-based diversification inferences, as, for instance, shown in insects (8). Therefore, we decided to assign sub-epoch ages to the SALMA-associated occurrences (**Fig. S1-2**), ensuring ourselves to sample the whole study period more evenly. As illustrated by many studies (2, 9), the taxonomic scale impacts fossil-derived diversification patterns. Defining species in the fossil record is difficult and prone to debate, and working at the species scale is particularly sensitive to biases such as synonymy or missing open literature elements (*e.g.*, 'cf.', 'aff.', etc.). Therefore, we analyzed our mammalian fossil database both at the genus and species levels (**Fig. S2**), but privileged the genus scale for our macroevolutionary conclusions. We further applied several treatments to our data. First, we tested the effect of removing singletons because our

genus-level and species-level occurrence datasets comprise 36% and 54% of singletons, respectively (*i.e.*, taxa only represented by a single occurrence in the entire dataset; **Tab. S1**). It is worth noting that including singletons in diversification inferences is still under debate (10–12). Also, PyRate was validated using simulated data with a proportion of singletons that, to our knowledge, never exceeded 34% (13). Hence, we possibly ignore how the model might behave with such high proportions of singletons as those we have, though it was found to be robust against data incompleteness. Second, we did not allow a given genus (or species) to have geographically and temporally-identical occurrences (as done by ref. (10)). Next, in order to have a better view on the different tempos of diversification between tropical and extratropical biomes, we assigned each occurrence a tropical or extratropical affinity. Traditionally – both when dealing with extant or fossil lineages – such a geographic splitting is made by defining a latitudinal threshold above (or under, depending on the hemisphere) which occurrences are considered tropical. The latter is commonly set as -23.4° in latitude, but sometimes also -23°, -23.5° or even -30°. However, such a threshold is unsatisfactory, mainly because it does not consider tropics' expansions and contractions through geological times (see refs. (14, 15) for a discussion on the topic). Therefore, based on their middle age, we binned our occurrences into 5-Myr time bins and reconstructed their paleocoordinates (using the mid age of the bin as reconstruction age) with the PALEOMAP Global Plate Model (16). Paleorotations were produced via an access to the GPlates Web Service (https://gwsdoc.gplates.org/) API implemented in the `paleorotate` function of the paleoverse R package (6). Then, to assign them a tropical/extratropical affinity, we overlaid these point data with Köppen-Geiger paleoclimate zones produced every 5 My (14, 17). Finally, our fossil occurrence data came with "diet" assignments, derived from dental ecomorphotypes, which we further revised and collapsed to only keep four different classes: carnivorous, herbivorous, insectivorous, and omnivorous.

Bayesian inference of diversification accounting for preservation

We used the Bayesian framework of fossil-based diversity and diversification inference accounting for preservation implemented in PyRate v.3 (18, 19). Relying on birth-death and preservation processes, PyRate jointly estimates the times of origination and extinction and the preservation rate of each taxon, as well as the origination and extinction rates of the underlying birth-death process. We approximated the posterior distribution of each parameter through Reversible-Jump Markov Chain Monte Carlo (RJMCMC) (13). The RJMCMC algorithm provides an objective estimate of the number of diversification rate shifts, but empirical case studies found that it could also be sensitive to gaps in the fossil record (8). Hence, we also analyzed our fossil dataset under a Birth-Death model with Constrained rate Shifts (BDCS) (20). In the BDCS model, origination and extinction rates can only vary in a piecewise-constant way between a predefined set of time bins. Given the temporal heterogeneity of our data (**Fig. S1** and **S4**), this framework was particularly relevant to us because the BDCS model can smooth rates through time when rates are very different within a bin due to preservation issues. We both tested geological stages and 5 My-long intervals as input bins. To achieve convergence, when working with full datasets, we ran 50,000,000 iterations at the genus level and 100,000,000 iterations at the species level, and sampled every 50,000. When working with taxonomically- or diet-specific datasets, we ran 20,000,000 iterations, sampling every 20,000. For each tested condition, we ran PyRate on 10 or 20 datasets of independently-sampled ages and retained those of which the majority of the parameters (posterior above all) converged. Parameters were considered convergent when their Effective Sample Size (ESS) was above 200. Convergence checks were assessed thanks to the PyMC 5.9.2 python library (21). For each set of runs, burn-in value was specified in an automatized pipeline as the value maximizing the ESS of the parameters (choosing between 1%, 5%, 10%, 25% and 50% of the posterior distribution), rather than using the same fixed value every time. Parallel computing

was made possible thanks to the parallel software (22). In the RJMCMC analyses, we allowed for a minimal time window between two origination/extinction rate shifts of 1 My (`-mindt 1`). We also allowed for preservation rate heterogeneity across taxa (`-mG`) as it is more realistic to consider uneven preservations across lineages (some lineages undergo better preservation than others). We set Gamma priors of shapes 1.1 (default value) and model-estimated rates for both origination and extinction rates (`-pL 1.1 0` and `-pM 1.1 0` options). The preservation rate prior was also sampled in a Gamma distribution of model-estimated rate, but we put a slightly larger shape (`-pP 2 0`), offering more flexibility (10). We assessed the most suitable preservation model for our data using the maximum-likelihood based model selection test included in PyRate (`-PPmodeltest` option), which resulted in favor of the Time-dependent Preservation Process (TPP) model allowing rate shifts between every geological stage (**Fig. S5-S6**). Last, we tested for the sensitivity of our analyses to singleton removal (`-singleton 1` option) (**Fig. S12-S13**). As the BDCS model takes longer to run than the RJMCMC model, we ran the former directly based on the origination and extinction times (respectively Ts and Te) table estimated with the latter (`-d` option). In fact, the joint estimation of Ts, Te and the preservation process is the same between both models. What changes is the diversification (birth-death) model they fit to the reconstructed diversity to assess the origination and extinction rates through time (λ and μ, respectively). BDCS models were run across 10,000,000 iterations, sampling every 10,000. All subsequent analyses were performed in R v4.4.0 (23).

Age-Dependent Extinction

To assess the effect of taxon age on its extinction probability, we fitted the Age-Dependent Extinction (ADE) model to our data (`-ADE 1` option in PyRate) (24). This model assumes that taxon extinction probability is only a function of its age, and fits a Weibull probability density to the extinction rate de-novo estimated from occurrence data. The presence (or not) of an ADE in our data is given by the value of the shape (ϕ) parameter of the Weibull function: if $\phi > 1$, extinction probability increases with taxon age; if $\phi < 1$ extinction probability decreases with taxon age; and if $\phi = 1$, no ADE can be characterized. In practice, we consider that the shape parameter significantly differs from one when one is not included in its 95% HPD. We ensured to fit this model within time windows with a relatively constant extinction rate. As we only retrieved one significant shift in extinction rate around 39 Ma (**Fig 1** and **S8-11**), we therefore investigated the effect of the ADE between 56 and 39 Ma, and between 39 and 23.03 Ma (`-filter` option) (**Fig S41**). Just like in the previous section, we set a time-variable preservation process (`-qShift` option) and allowed for preservation rate heterogeneity across taxa (`-mG` option). We ran the model for 40 million MCMC generations and sampled every 40,000 iterations. Parameters were considered convergent when their ESS was above 200. Convergence checks were achieved using the PyMC3 python library (21).

Dissimilarity across time among faunal assemblages

To quantify the extent to which our successive faunal assemblages differed from one another, both in terms of taxonomic and trophic composition, we computed two commonly-used dissimilarity indices to compare ecological communities. We used Jaccard's similarity index to compare the taxonomic composition of the five main mammal subdivisions we defined (notoungulates, other native ungulates, rodents, xenarthrans, and metatherians). Considering $n(E)$ and $n(O)$ the total number of taxa within Eocene and Oligocene faunas, respectively, and $n(E \cap O)$ the number of shared taxa between both assemblages, this index is simply expressed as:

$$J = \frac{n(E \cap O)}{n(E)n(O)}$$

This index is very intuitive and does not require any knowledge about the abundance of each taxon within both communities. It ranges from zero to one, and the closer it gets to one, the more similar the two assemblages compared are. Conversely, we compared sub-epoch-level functional compositions of the mammal assemblages by using the Bray-Curtis dissimilarity index, accounting for variations in relative abundance among the four trophic classes we defined based on dental ecomorphotypes (carnivorous, herbivorous, omnivorous, and insectivorous). Considering two assemblages A and B, p classes (here, $p = 4$), and $n(A, i)$ and $n(B, i)$ the respective numbers of taxa belonging to the class i within the assemblages A and B, this index is expressed as:

$$BC = 1 - \frac{2\sum_{i=1}^{p} min(n(A,i), n(B,i))}{\sum_{i=1}^{p}(n(A,i) + n(B,i))}$$

It also ranges from zero to one, but in that case, values closer to one indicate increasingly dissimilar assemblages.

Multivariate Birth Death (MBD) model and Selection of environmental variables

To assess the impact of environmental factors on the diversification patterns of SAMs during the EOT, we ran a Multivariate Birth-Death (MBD) model in PyRate (25). This model carries out two independent correlations involving a set of environmental covariates (that can be biotic and/or abiotic) and diversification rates newly-estimated from empirical T_s and T_e: one with the origination rate (λ), and the other with the extinction rate (μ). Each variable is therefore assigned to two correlation coefficients, one for the correlation with λ ($G_{\lambda,i}$, where i is the index of the variable in the set of covariates) and the other for the correlation with μ ($G_{\mu,i}$). An MCMC algorithm jointly estimates baseline origination and extinction rates and all the G_λ and G_μ, while controlling for over-parameterization. Each $G_{\lambda,i}$ and $G_{\mu,i}$ is assigned a shrinkage weight ($w(G_{\lambda,i})$ or $w(G_{\mu,i})$), ranging between 0 and 1, testing its significance – hence, the significance of the correlation itself. A correlation of coefficient $G_{\lambda,1}$ is considered significant if $w(G_{\lambda,1}) > 0.5$ and if a sufficiently high proportion of its posterior density does not overlap with 0. We selected seven abiotic and one biotic variable that appeared relevant to our case study (**Tab. S2**). The abiotic variables included two global and four local-scale ones. Temperature is known for being a major actor in the diversification of a wide range of clades (*e.g.*, 26). Hence, we included in our model the average Cenozoic temperature dataset assembled by ref. (27), using atmospheric $\delta^{18}O$ and $\delta^{13}C$ records from ref. (28). In addition, as they are expected to play a key role in habitat fragmentation on macroevolutionary scales, we added global sea level trends (29) and the average Andean uplift (30). We also added the Neotropical plant diversity dataset assembled (31). Last, there is a debate regarding the role of land opening in shaping the evolution of SAM faunas, notably among herbivores. We therefore included two regional proxies for land opening: Patagonian patterns of relative abundance of open habitats (32–34) and Patagonian relative leaf area index (35). Each abiotic correlate was subsampled or interpolated to a 500 ky time step. In addition, we tested for diversity-dependence effects that could either come from the diversity of the tested clade itself (self-diversity, `-rmDD 0` option) or other clades (allowing to hypothesize possible inter-clade interactions). As we expected environmental dissimilarities between the Eocene and the Oligocene at the continent scale, especially in high latitudes (where most of our occurrences come from), we did not expect Eocene and Oligocene faunas to have the same environmental constraints. That is why, in addition to searching for environment signature in the diversification pattern across all our study period, we also decoupled trends among post-early Eocene Climate Optimum Eocene faunas (51–33.9 Ma), and Oligocene faunas (33.9–

23.03 Ma). Each MBD model was run across 10,000,000 iterations, sampling every 10,000. We only carried out exponential correlations (`-m 0` option). Convergence of the parameters was assessed using the pymc 5.9.2 Python library (21), and parameters were considered convergent if their ESS were greater than 200. A summary of our entire methodological pipeline is provided in **Fig.S2**.

Considering the reliability of crowdsourced data

Over the past few decades, massive efforts have been devoted toward centralizing all published fossil data into large databases (*e.g.*, https://nowdatabase.org/, https://paleobiodb.org/, https://www.neotomadb.org/). Such an amount of easily-accessible data provided the invaluable opportunity for scientists to investigate large-scale patterns and processes of biodiversity using fossils, the only direct evidence of life in the past. In our case, our primary source of data came from The Paleobiology Database (https://paleobiodb.org/). However, we spotted many errors in the raw data, mostly regarding occurrences' age or taxonomic name (typos, unaccounted synonymies, missing open nomenclature elements, etc.). Most of these errors could not have been detected, and further corrected, without the authors' prior knowledge on the group (see **Fig. S2** and **S4**). The need for occurrence data revision was already illustrated by ref. (36), who pointed out significant differences when carrying out diversification analyses from uncleaned and cleaned occurrence data. Therefore, we argue that although powerful statistical tools exist, tackling macroevolutionary issues cannot be done without preliminary biological knowledge on the focal group.

2. Manual cleaning details

In this part, we provide some details on the Paleogene fossil occurrence cleaning effort we carried out. All co-authors were involved in this part, and some changes have not been documented. Our raw and final datasets can be found attached with this manuscript. Computer-supervised cleaning steps are documented in our GitHub repository (https://github.com/Buffan3369/Neotropical_mammals.git).

The age ranges of the occurrences belonging to the Paso del Sapo fauna (Western Patagonia, *"Sapoan fauna"* SALMA) were set close to the Ypresian–Lutetian boundary. More precisely, occurrences from the *La Barda* or the *Laguna fría* localities were respectively set to 45-47 Ma and 48-49 Ma (37).
Occurrences assigned to the former *Casamayoran* SALMA were re-assigned to a Middle Eocene age (37.71-47.8 Ma), except when more precision was provided in subsequent studies (*i.e.,* radiochronological dating)

Astrapotheria

Grypolophodon imperfectus (coll. nb. 176290, (38)) was removed as nomen dubium.
Parastrapotherium holmbergi (coll. nb. 176290, (39)) formation was set to Sarmiento, stage to Deseadan–Colehuehuappian, and age range to 20–29 Ma.
Xenastrapotherium sp. (coll. nb. 55602, (40)) and *Xenastrapotherium amazonense* (coll. nb. 55602, (41)) were reassigned to Laventan stage (11.8–13.8 Ma) according (42).
Notorhinus denticulatus (coll. nb. 176290, (39)) removed as nomen dubium. *Astrapotherium* (coll. nb. 50074, (43)) re-assigned to Santacrucian.

Stem Metatheria

Wirunodon chanku (coll. nb. 149523, (44)) age range was set to early Oligocene (28.7–33.9 Ma). The three occurrences of the *Rumiodon* genus were attributed to early Oligocene (28.7–33.9 Ma) All occurrences of the *Protodidelphis* genus were attributed to late Paleocene-early Eocene (47.8–59.2 Ma), just like all occurrences from the *Carolopaulacoutoia* and *Didelphopsis* genera.
Marmosopsis sp. (coll. nb. 133039, (37)) age range was set to Late Paleocene-early Eocene (47.8–59.2 Ma).

Cingulata

Added one occurrence of *Eosclerocalyptus* (6.4–6.6 Ma), *Doellotatus chapadmalensis* (5.9–6 Ma) and *Macrochorobates scalabrinii* (6.4–6.6 Ma) from the Maimará formation, Maimará locality, Jujuy, Argentina (45).

Didelphimorphia

Added one occurrence of the extant genus *Chacodelphys* (46).
All occurrences assigned to the *Micoureus* genus were re-assigned to the *Marmosa* genus, the former being a sub-genus of the latter (47).
Based on (48), we added a new occurrence of *Marmosa* in the TAR-31 locality of Shapaja, Peru, late Middle Miocene (11.67–15.63 Ma).
Paradidelphys sp. (coll. nb. 157795, (49)) was synonimized with *Thylophorops* (50).
Added one occurrence of *Thylamys* cf. *colombianus* from the TAR-31 locality of Shapaja, Peru (47).
Added one occurrence of *Sparassocynus maimarai* from the Maimará formation, Maimará locality, Jujuy, Argentina (45).

Didolontidae (SANU family with uncertain affinity)

Archaeohyracotherium mediale (Didolodontidae, coll. nb. 176164, (38)) was synonimized with *Asmithwoodwardia subtrigona* (Protolipternidae) by ref. (51).
Argyrolambda conidens was synonimized with *Didolodus multicuspis* (51).
Didolodus sp. (coll. nb. 199563, (52)) was removed as associated to “unidentified Didolontidae” in the paper.

Litopterna

Enneoconus parvidens (coll. nb. 176164, (53)) was synonimized with *Ernestokokenia nitida* by ref. (51).

Microbiotheria

Clenia brevis was excluded from the *Clenia* genus by ref. (54). Hence, we rename the genus aff. *Clenia*.

Notoungulata

All occurrences referred to as *Bryanpattersonia nesodontoides* were synonimised with *Archaeotypotherium propheticus* according to (55).
All occurrences referred to as *Bryanpattersonia sulcidens* were renamed *Protarchaeohyrax gracilis* according to (55). All occurrences of *Anisotemnus distentus* were assigned to Middle Eocene (37.71-47.8 Ma) according to (56). Removed two occurrences of *Archaeotypotherium propheticus* (coll. nb. 176286), absent from the original publication (38). Age range of *Coelostylodon florentinoameghinoi* and *C. caroloameghinoi* (coll. nb. 13779) was set to Barrancan (39-41.7 Ma), in line with the original reference. Assign all *Eomorphippus obscurus* occurrences described in Simpson (38) (coll. nb. 38653) a Mustersan age (35-38.2 Ma).

Paucituberculata

Acdestodon genus was synonimised with *Acdestis* (57). Added one occurrence aff. *Palaeothentes* from the TAR-31 locality of Shapaja, Peru (47). *Propalaeothentes* was synonimised with *Palaeothentes* (57). Added *Palaeopanorthus primus* from the Colhuehuappian of Chubut, Argentina (57).

Pilosa

Added one occurrence of *Proscelidodon* (Upper Miocene-Lower Pliocene) and one cf. *Pleurolestodon* (5.8–5.9 Ma) from the Maimará formation, Maimará locality, Jujuy, Argentina (45).

Polydolopimorphia

Chulpasia sp. (coll. nb. 132938, (58)) was removed as only one record of *Chulpasia* (species *mattaueri*) has been found in Peru.
Groeberia minoprioi (coll. nb. 92669, (59)) age range was set to late Eocene-early Oligocene (27.82–37.71 Ma). *Patagonia peregrina* (coll. nb. 27311, (54)) age range was set to Chattian (23.03–27.82 Ma). All occurrences of *Polydolops clavulus* were renamed *Archaeodolops clavulus*, according to (60). Added one occurence of *Archaeodolops clavulus*, according to the same paper.
All occurrences of *Proargyrolagus bolivianus* were attributed to the Salla formation, Bolivia. Hence, their age boundaries were restricted to 24.5–26 Ma.
Amphidolops serrula (coll. nb. 13779, (61)) was re-assigned to Late Paleocene (oldest recorded Polydolopid).
Polydolops sp. (coll. nb. 14208, (62)) was removed as age boundaries (Early Miocene) were way outside known boundaries for records of this genus (Middle Eocene).
Added occurrence from a newly described genus of the Prepidolopidae family from the TAR-74 locality of San Martín, named Prepidolopidae *gen_A* (52).

Primates

Ages of Deseadian soriacebines *Branisella* and *Canaanimico* were restricted to the 24.5–26 Ma interval according to (63).

Pyrotheria

Re-assigned the four occurrences of *Griphodon* described in refs. (64) as cf. *Griphodon* sp1 to sp4.

Rodentia

We should mention that all the rodents considered in this study belong to the order Caviomorpha, and arrived in the South American landmass in the middle Eocene (65). ***Added Occurrences***
Ricardomys longidens, Laventan age, San Martín department, Peru (66).
Microscleromys sp. (two occurrences), *Microscleromys cribriphilus*, *Microscleromys paradoxalis*, *Microsteiromys jacobsi*, *Nuyuyomys chinqaska*, *Scleromys*, Laventan age, San Martín department, Peru (66).
Balsayacuy sp., Rupelian age (restricted to the 27.82–31.1 Ma interval), Departamento de Ucayali, Santa Rosa locality, Peru (67). Described as an occurrence of *Balsayacuy huallagaensis*, but species attribution doubtful. Hence, restricted to genus level. From the same paper (same locality and same age), we also add one occurrence of *Shapajamys minor*, one of *Ucayalimys amahuacensis* and one of *Vucetichimys pterilophodonica*.
Erethizon sp., Vorohuean (Marplatan) age, Uquía formation, Quebrada de Humahuaca locality, Jujuy state, Argentina (68).
Eoincamys valverdei and *Tarapotomys subandinus*, early Oligocene of respectively TAR-72 and TAR-22, San Martín, Peru (69).
?Palaeocavia (5.8–5.9 Ma), *Pithanotomys? solisae* (5.8–5.9 Ma), *Pithanotomys* sp. (5.8–5.9 Ma) *Palaeocavia* sp. (5.9–6.0 Ma) and *Palaeocavia humahuaquense* (6.4–6.6 Ma) from the Maimará formation, Maimará locality, Jujuy, Argentina (45).

Corrections
Cachiyacuy contamanensis (coll. nb. 149523, (70)) was renamed *Cachiyacuy* sp. as taxonomic assignation is under debate. Two *Cachiyacuy contamanensis* occurrences from the same collection, same paper, were renamed cf. *Cachiyacuy contamanensis*, for the same reason.
Kichkasteiromys raimondii: age range set to 34–35 Ma.
Time boundaries of *Cachiyacuy* cf. *contamanensis* and *Cachiyacuy contamanensis* (coll. nbs. 207061 and 207062, (71)) were set to Priabonian (33.9–37.2 Ma). Same for *Cachiyacuy* cf. *kummeli*, *Eoespina* and cf. *Eoespina* (coll. nb. 207062, 207062 and 207065, (71)) Remaining occurrences of the genus *Cachiyacuy* (four in total) were set to late Eocene (33.9–41.2 Ma).
Canaanimys maquiensis (coll. nb. 149523, (70)) was renamed *Canaanimys* sp. as taxonomic assignation under debate.
Time boundaries of four *Cachiyacuy kummeli* occurrences (coll. nb. 144474, (65); 176136, (72), 207067 and 207062 (71)) were set to Bartonian-Priabonian (33.9–41.2 Ma). Same for *Eobranisamys* sp. (coll. nb. 176151, (72)) and for all occurrences from the 144474 collection, including one *Chachapoyamys* cf. *kathetos* (66), one *Eoespina* sp. (65), one *Canaanimys maquiensis* (65) and one *Eobranisamys javierpardoi* (72).
Ages of all occurrences from the collection 149523 were restricted to Rupelian. These included two cf. *Cachiyacuy kummeli* occurrences (70), one *Canaanimys* sp. (70), one *Eobranisamys riverai*, one *Eobranisamys romeropittmanae*, one *Eoespina woodi*, one *Eoincamys ameghinoi*, one *Eoincamys pascuali*, one *Eopicure kraglievichi*, one *Eosachacui lavocati*, one *Eosallamys paulacoutoi*, one *Eosallamys simpsoni* (73), one *Pozomys* sp., two *Pozomys ucayalensis* (70), one *Eodelphomys almeidacomposi*, one *Eopululo wigmorei* (73).

Ages of two *Sallamys pascuali* occurrences (coll. nb. 95688, (74); 133539, (75)), three *Branisamys luribayensis* (coll. nb. 95688 (74); 95688 (76); 133539 (75)) were sharpened to the 25–26 Ma interval.
Ages of one *Pozomys ucayalensis* (coll. nb. 176129, (72)) were set to Bartonian-Priabonian (33.9–41.2 Ma). Ages of two *Eoespina* sp. occurrences (coll. nb. 176140, (72)) was restricted to late Eocene.
Ages of one *Eoespina* and one cf. *Eoespina* occurrence (coll. nb. 207062 and 207065, (71)) were set to Rupelian.
Eoincamys pascuali (coll. nb. 207064, (71)) was renamed *Eonincamys* sp. Age range of all Late Oligocene occurrences from the Salla formation, La Paz, Bolivia, was set to 24.5–26 Ma. *Eopululo wigmorei* (coll. nb. 225588, (52)) species name was set to *Eopululo* sp. according to (66).
Names of all *Eumysops chapalmalensis* occurrences were set to *Eumysops chapadmalensis*.

Removed occurrences
Cachiyacuy kummeli (coll. nb. 207067, (71)), renamed *C.* cf. *kummeli* (doublon) according to (66).
Canaanimys sp. (coll. nb. 176136, (64)), taxonomic revision (66).
Canaanimys maquiensis (two occurrences, coll. nb. 207066 and 207067, (71)), taxonomic revision (66).
Chachapoyamys kathetos (coll. nb. 207067, (66)), re-assigned to *C.* cf. *kathetos* (doublon) (66).
Four Brazilian occurrences of the genera *Eobranisamys* (two) and *Eoincamys* (two) with ages for being rework (coll. nb. 57989, (77); coll. nb. 217834, (78)).
Tarapotomys sp. (2 occurrences) (coll. nb. 199560, (69); coll. nb. 199563, (52)), respectively re-described as aff. *Tarapotomys* sp. and *Tarapotomys subandinus* in (66).
Incamys bolivianus (coll. nb. 95688, (74)), doulon.
Asteromys bolivianus (coll. nb. 133591, (79)), doublon.
All *Rattus rattus* occurrences, as introduced by humans.

Sparassodonta

Cleaning was highly based on Tarquini et al. 2022 (2). In addition, we removed our single *Argyrolestes peralestinus* occurrence (coll. nb. 176285, (80)) as nomen dubium (81).

Supplementary figures

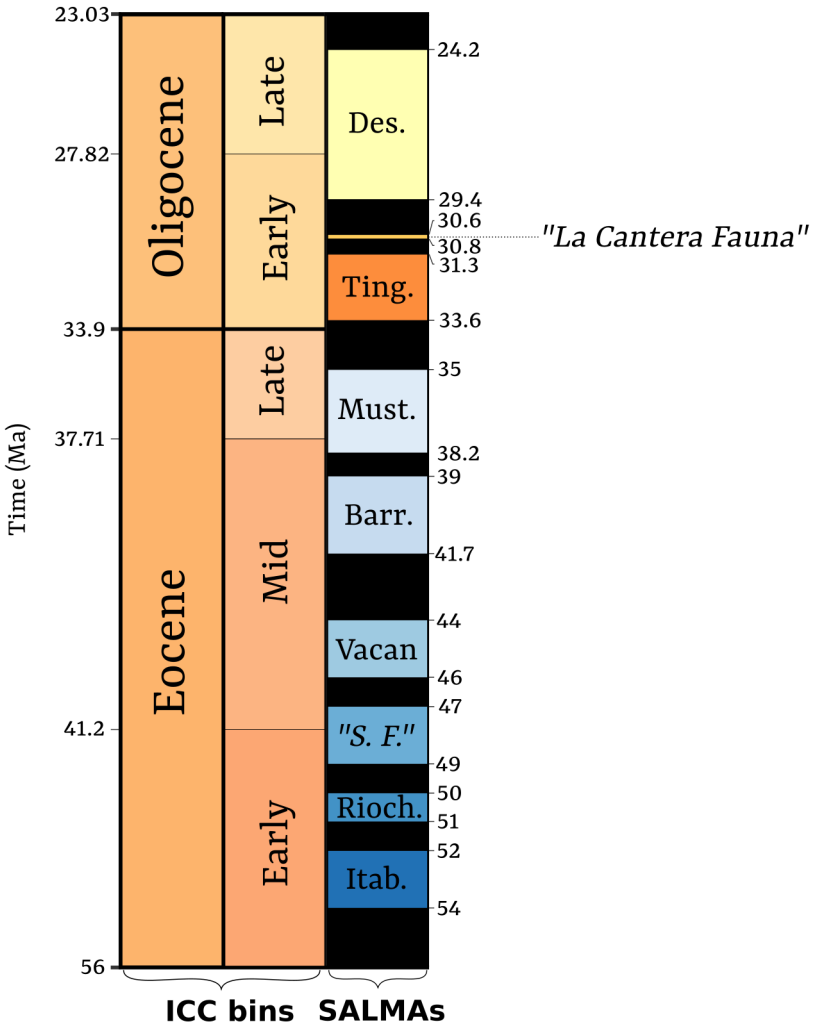

Supp. Figure 1: Time bins used in this study. Bins representing International Chronostratigraphic Chart 2022 (ICC bins) geological epochs (leftmost vertical band) and sub-epochs (middle vertical band), and representing South American Mammal Ages (SALMAs, rightmost vertical band) are depicted. SALMA boundaries were determined from Dunn et al. (2013), Woodburne et al. (2014) and Kouvari (2023). Note that an absolute estimate does not exist for the majority of them. Black rectangles stand for gaps in the South American mammalian fossil record. *Abbreviations for SALMAs. Des: Deseadan, Ting: Tinguirirican, Must: Mustersan, Barr: Barrancan, "S. F." : "Sapoan Fauna", Rioch: Riochican, Itab: Itaboraian.*

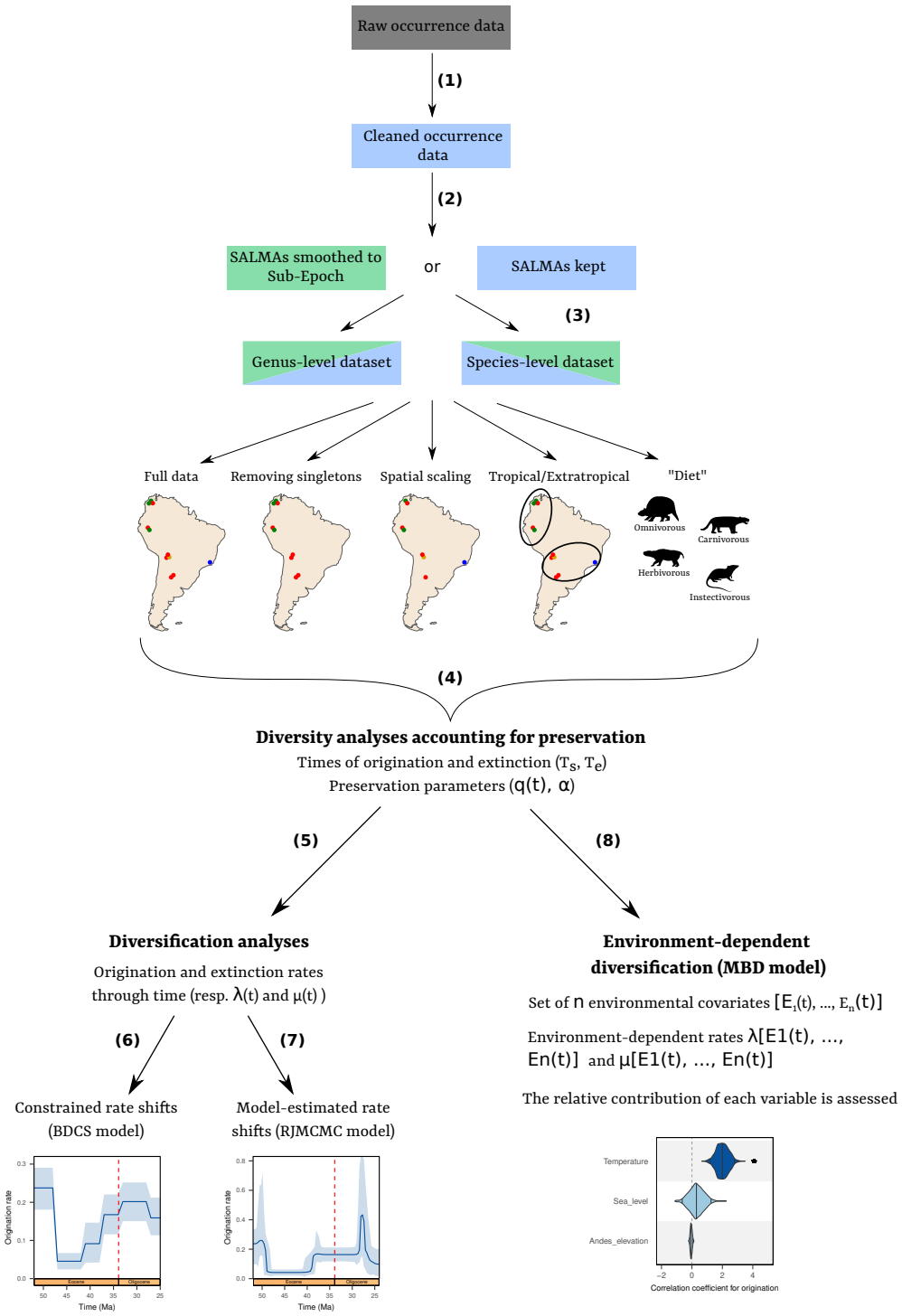

Supp. Figure 2: Schematic view of our data methodological pipeline.

We downloaded our data on The Paleobiology Database (https://paleobiodb.org/). We made sure to match each occurrences' time range with the boundaries of its corresponding interval, either being a geological stage/epoch (55% of our occurrences) or a South American Land Mammal Age (SALMA) (45% of our occurrences). Then, we cleaned the data, verifying for each occurrence its age range, taxonomic name (correcting synonyms), restoring missing elements of open nomenclature (*eg*., "?", "cf.", "aff."), removing duplicates and adding eventually newly-published data (1). Afterwards, occurrences associated to a SALMA were either binned to their corresponding sub-Epoch ('SALMA smoothed to Sub-Epoch') (**?**) or left as they were ('SALMA kept') (2). We also both analyzed diversification patterns at the species and the genus level (3). Several subsettings were tested, considering (i) full data, (ii) data without singletons, (iii) spatially scaled data, (iv) tropical partitioning and (v) "diet" (based on dental ecomorphotype). Once subsetted, each individual occurrence dataset was used as an input for our diversity inference accounting for preservation (4). Then, we proceeded to the diversification inference, either by (5) fitting birth-death models with constrained rate shifts (BDCS) (6) and model-estimated rate shifts (RJMCMC) (7) or by fitting environment-dependent multivariate birth-death models (MBD) (8). Last, we fitted an age-dependent extinction (ADE) model to our occurrence data within two time frames with constant extinction rate (9).

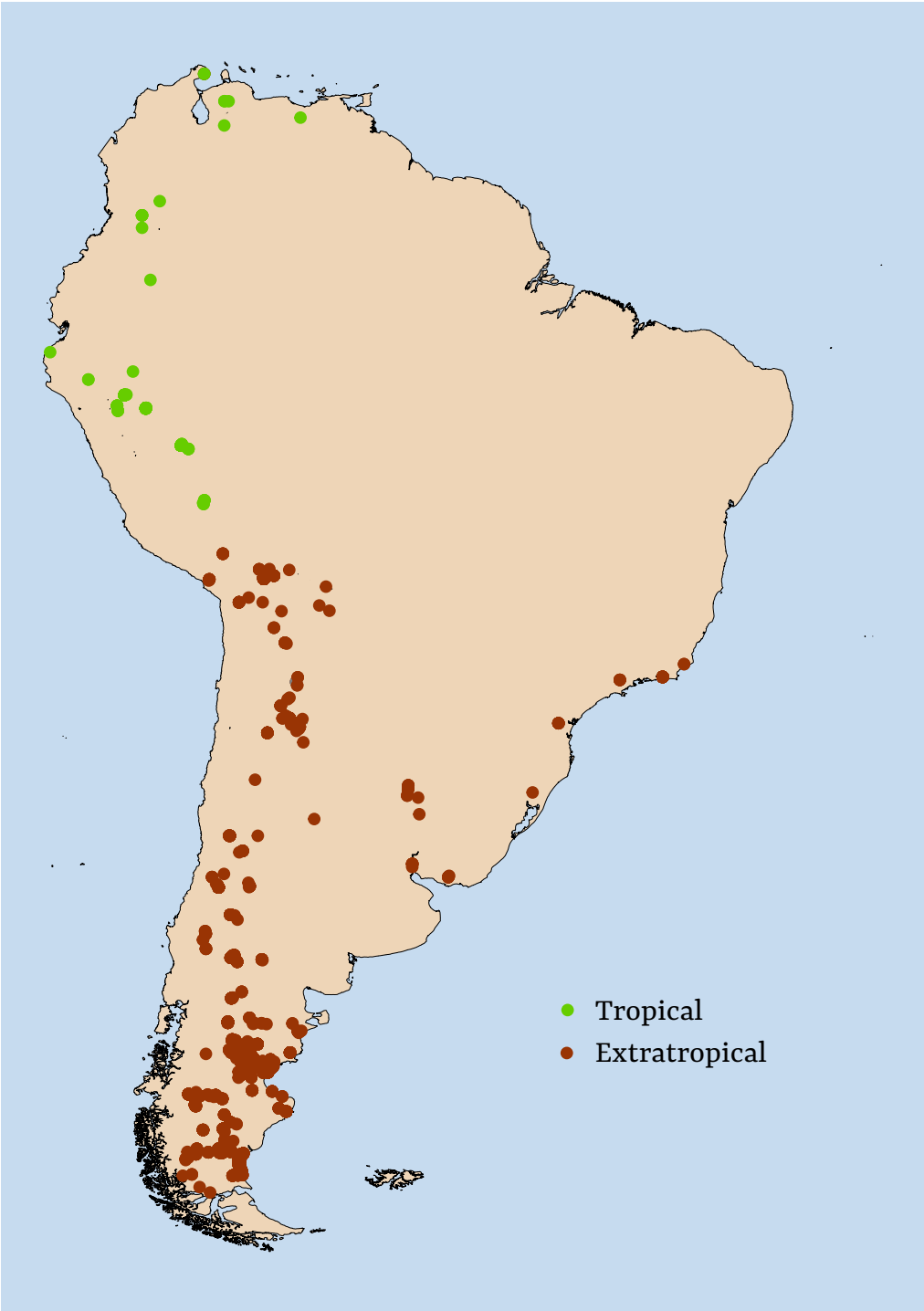

Supp. Figure 3: Map of the fossil-bearing localities considered in this study (435 collections).

These collections comprise a total of 3384 retained occurrences, including 156 of palaeotropical affinity (in green, 43 collections) and 3326 of extra-palaeotropical affinity (in brown, 391 collections).

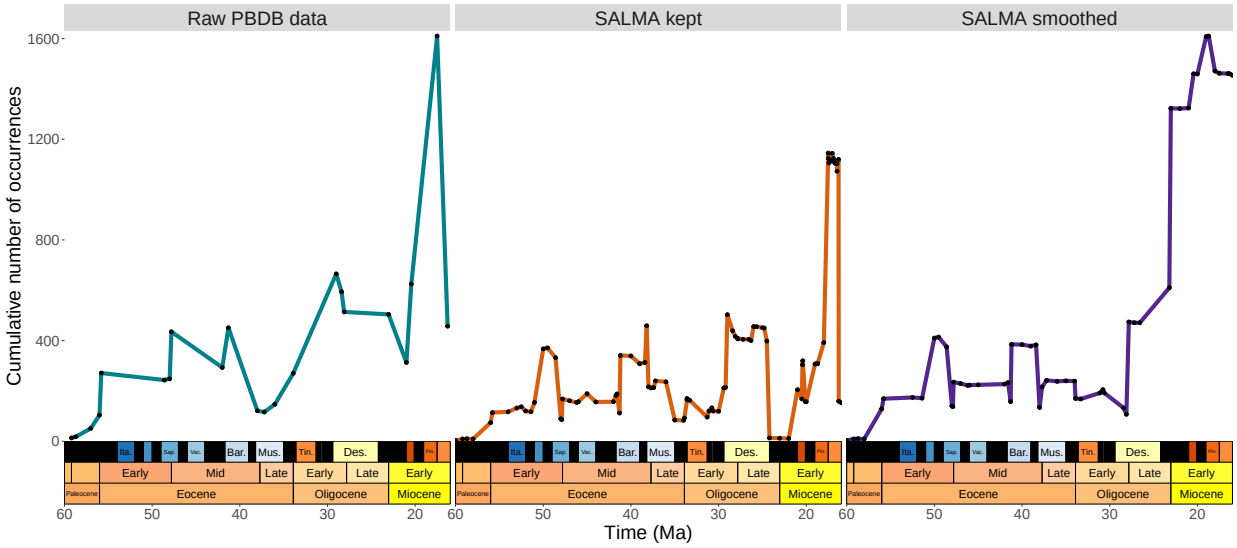

Supp. Figure 4: Cumulative number of occurrences through time within our study period. The cumulative number of occurrences is computed forward in time, starting from the lower age boundary of the oldest occurrence. Given a time t_1, this metric grows by the difference between the number of occurrences having t_1 as lower and upper boundaries. In practice, the times when this metric was computed are represented by the black dots. On the left, results from the raw data downloaded from PBDB are shown. In the middle, results from cleaned occurrences are shown. On the right, results from the same cleaned data but after smoothing occurrences associated to a South American Land Mammal Age (SALMA) to their corresponding sub-epoch (see **Fig. S1**) are shown.

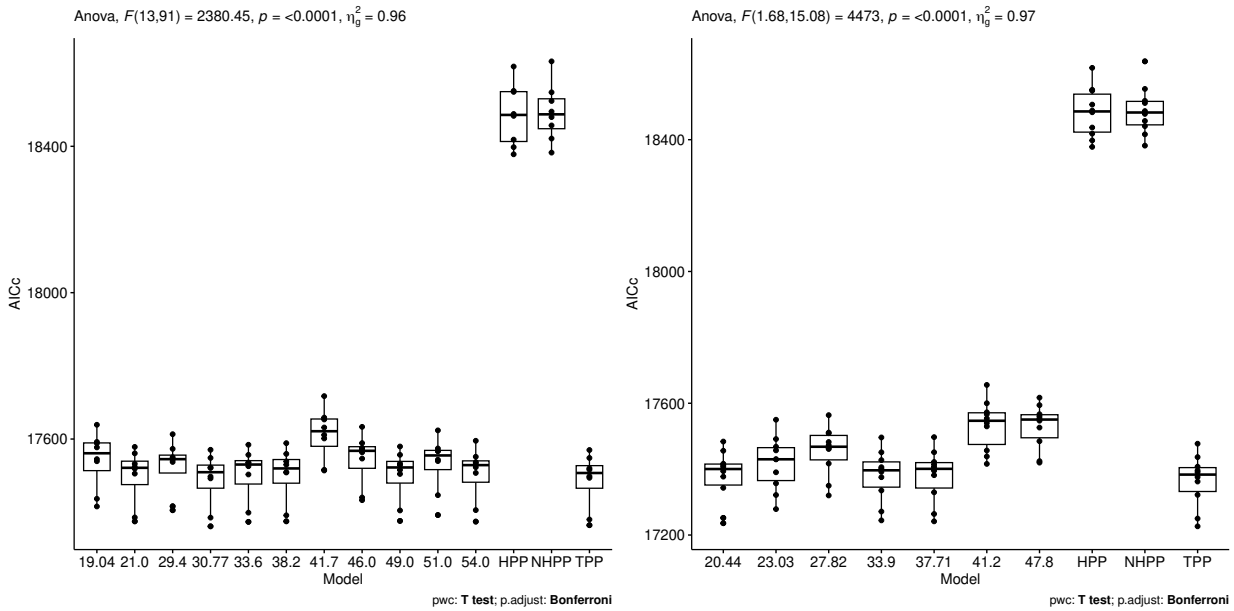

Supp. Figure 5: Preservation model selection under two TPP scenarios applied to the genus dataset with smoothed SALMAs. Models on the left of the x axis indexed by numbers are TPP with one removed bin, corresponding to the number. In the three cases, the lowest AICc is reached with the TPP model. Results were obtained on 10 replicates. (left) TPP with rate shift at every South American Land Mammal Age (SALMA) (mean AICc for TPP : 17486.42). (right) TPP with rate shift at every stage (mean AICc for TPP : 17364.53). Details for the AIC of all models can be found in Dataset S1.

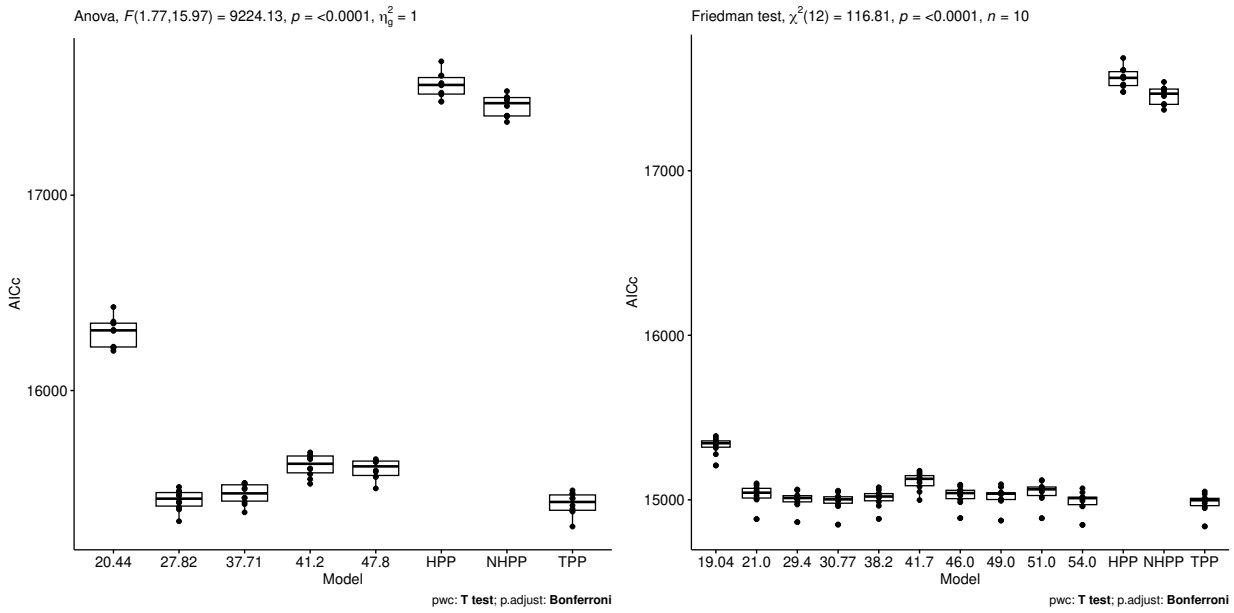

Supp. Figure 6: Preservation model selection under two TPP scenarios applied to the genus dataset without smoothing SALMAs. Models on the left of the x axis indexed by numbers are TPP with one removed bin, corresponding to the number. (left) TPP with rate shift at every stage (mean AICc for TPP : 15420.42). (right) TPP with rate shift at every SALMA (mean AICc for TPP : XXX). Details for the AIC of all models can be found in Dataset S1.

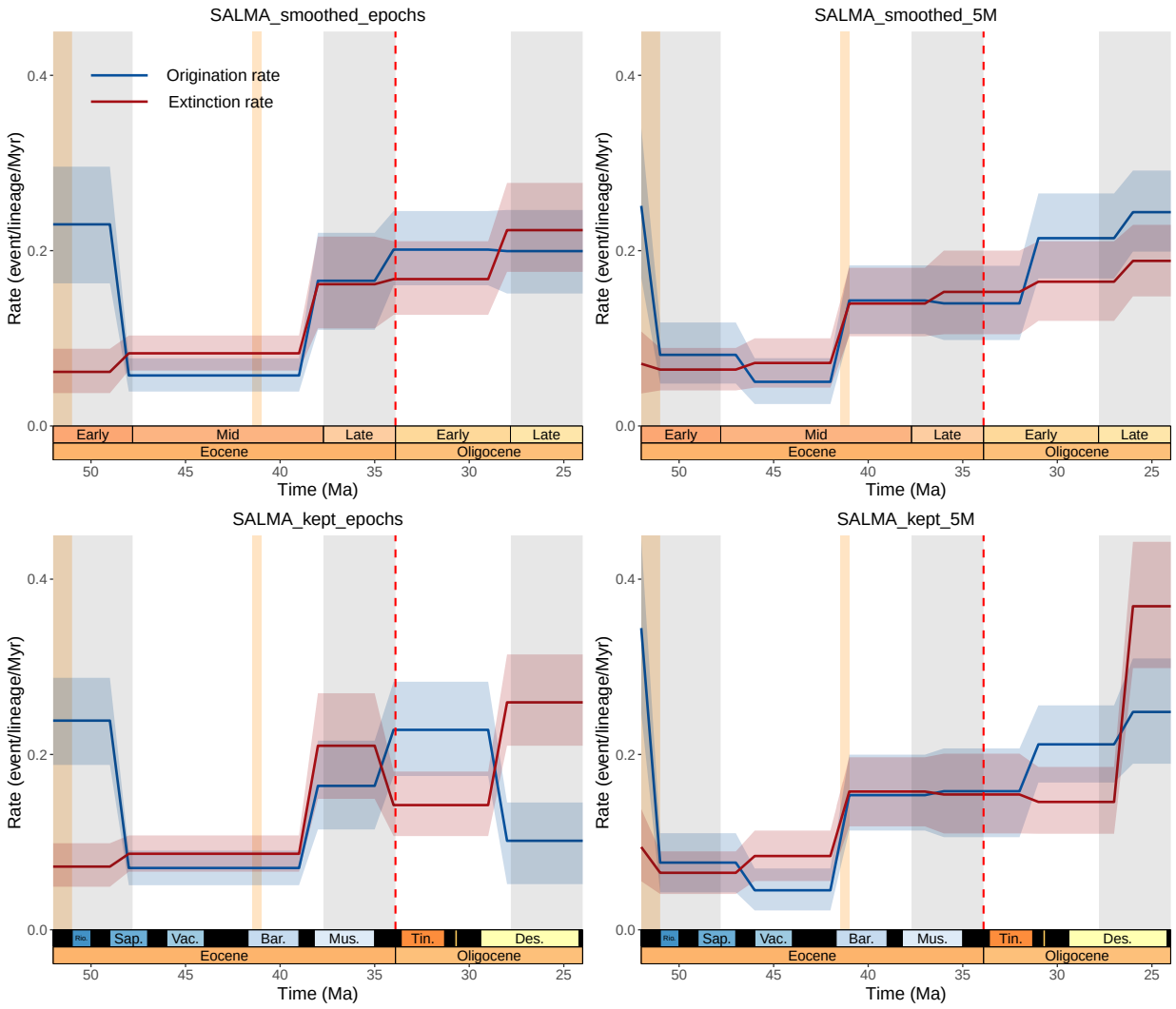

Supp. Figure 7: Diversification rates of our full dataset after (or not) smoothing SALMAs to their corresponding sub-Epochs, estimated under the BDCS model with two different time bins for rate shifts. Origination rates are displayed in blue and extinction rates in red. Solid lines show average rates, and shaded areas their corresponding 95% HPD. Light brown vertical bands respectively display the early Eocene Climate Optimum (EECO, 53-51 Ma) and the Mid-Eocene Climate Optimum (MECO, 42-41 Ma).

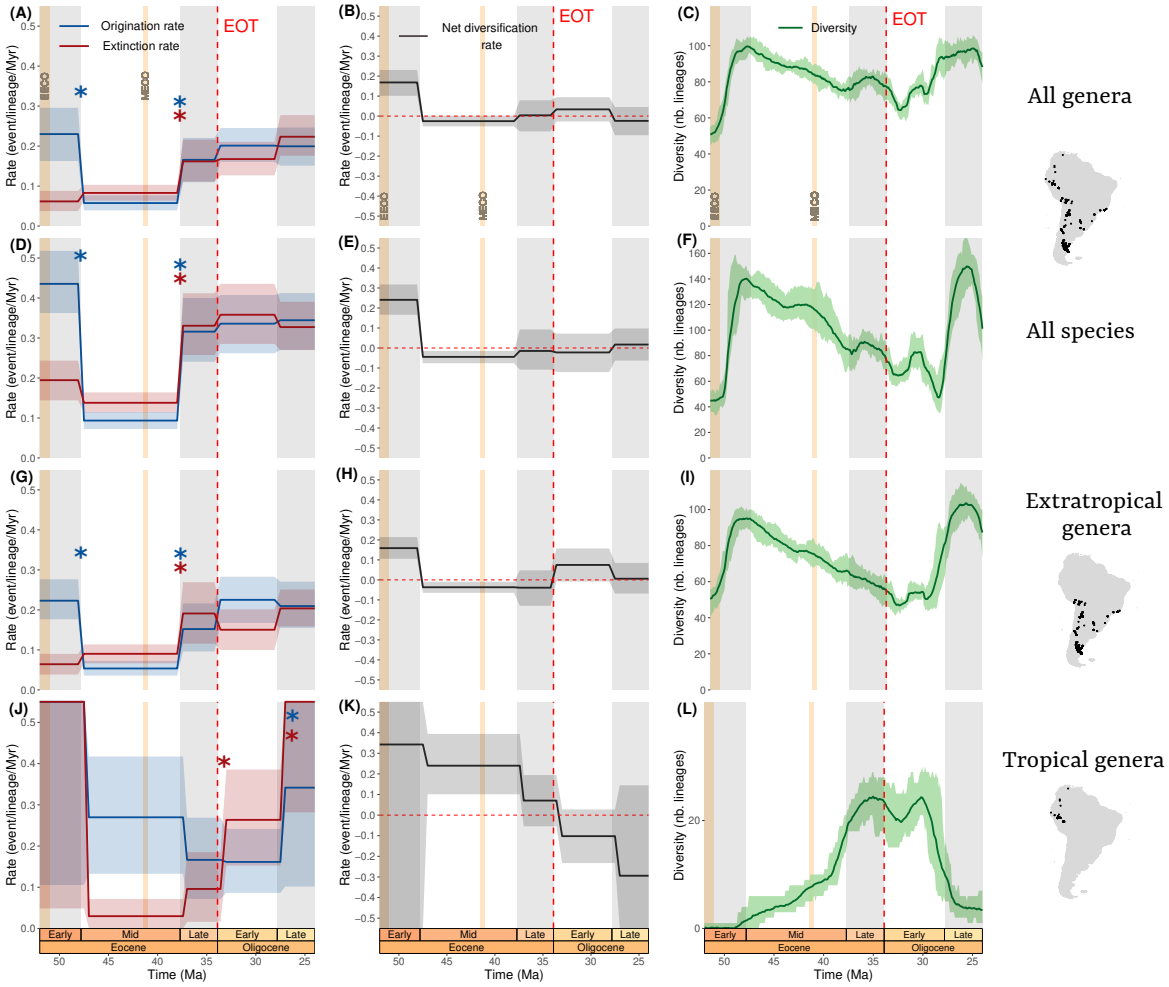

Supp. Figure 8: Diversification and diversity dynamics of South American Mammals from the early Eocene to the Late Oligocene. Trends are represented for all genera (A-C), all species (D-F), extratropical (G-I) and tropical genera (J-L). Light orange bands represent the early Eocene (53-51 Ma) and the Mid-Eocene (~41 Ma) Climate Optima, respectively abbreviated as EECO and MECO. Blue and red stars respectively represent significant shifts in origination and extinction rates.

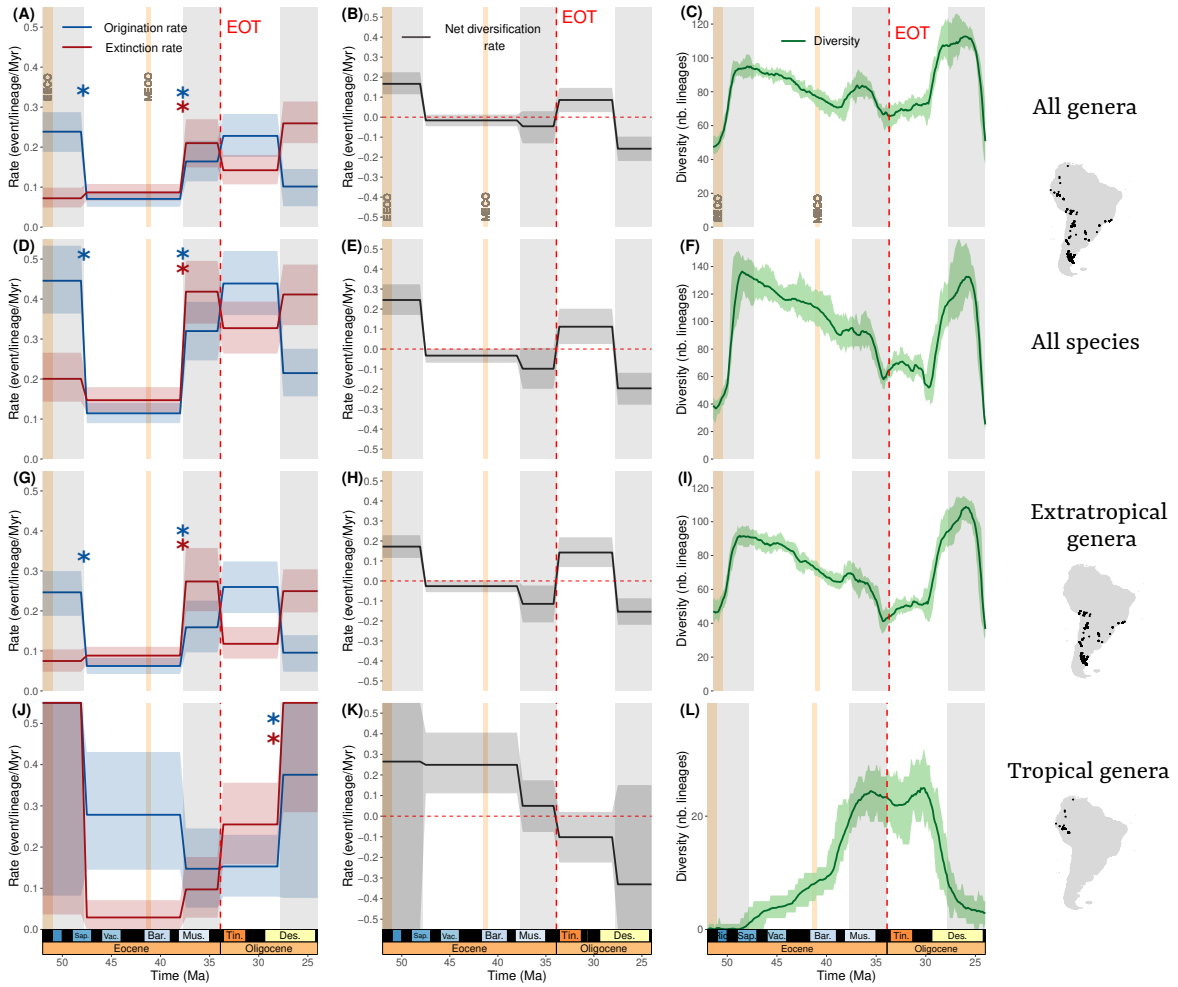

Supp. Figure 9: Diversification and diversity dynamics of South American Mammals from the early Eocene to the Late Oligocene without binning SALMAs to their corresponding sub-epochs. Trends are represented for all genera (A-C), all species (D-F), extratropical (G-I) and tropical genera (J-L). Light orange bands represent the early Eocene (53-51 Ma) and the Mid-Eocene (~41 Ma) Climate Optima, respectively abbreviated as EECO and MECO. Blue and red stars respectively represent significant shifts in origination and extinction rates.

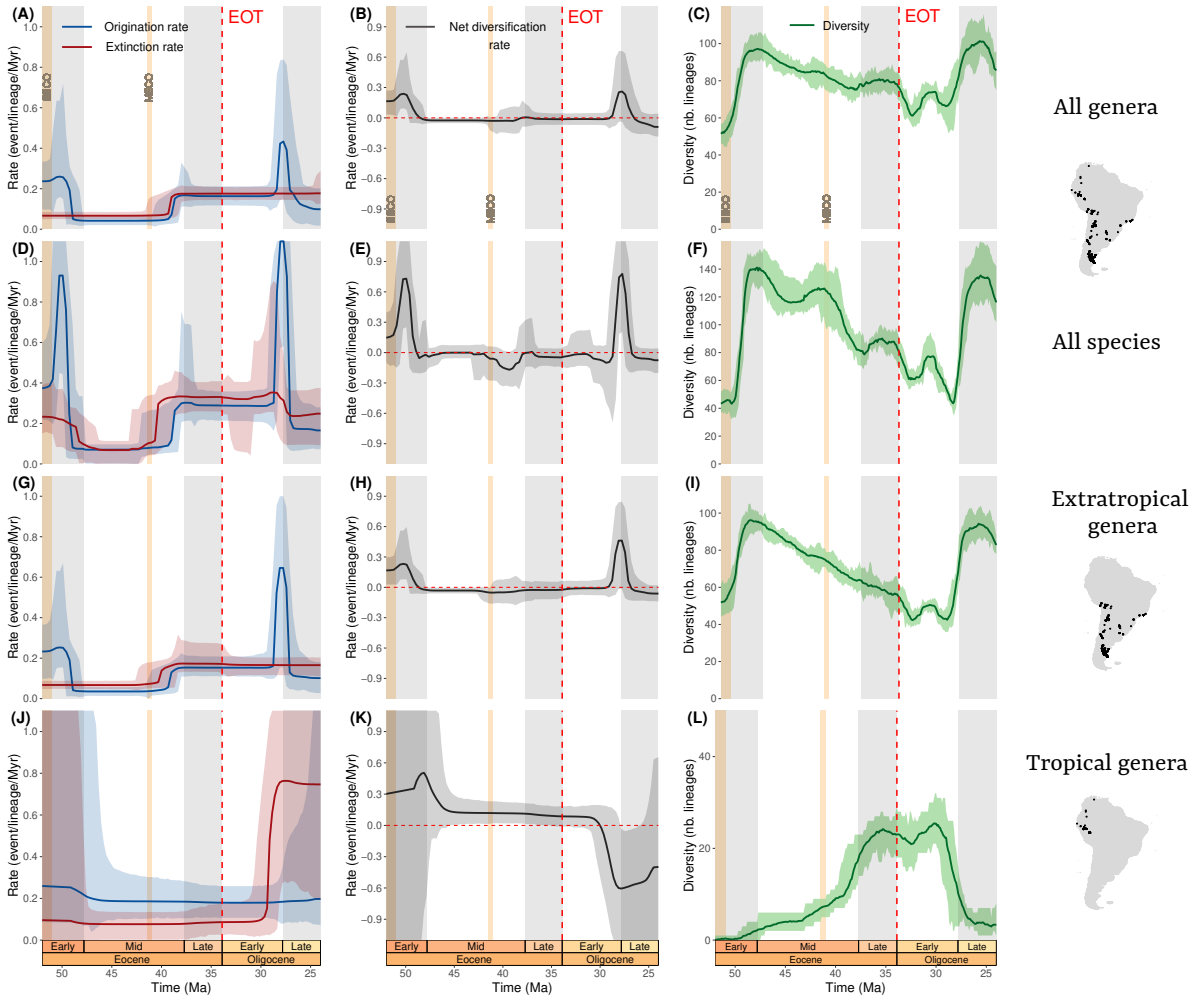

Supp. Figure 10: Diversification (estimated with RJMCMC) and diversity dynamics of South American Mammals from the early Eocene to the Late Oligocene (SALMAs binned to their corresponding Sub-Epochs). Trends are represented for all genera (A-C), all species (D-F), extratropical (G-I) and tropical genera (J-L). Light orange bands represent the early Eocene (53-51 Ma) and the Mid-Eocene (~41 Ma) Climate Optima, respectively abbreviated as EECO and MECO. Blue and red stars respectively represent significant shifts in origination and extinction rates.

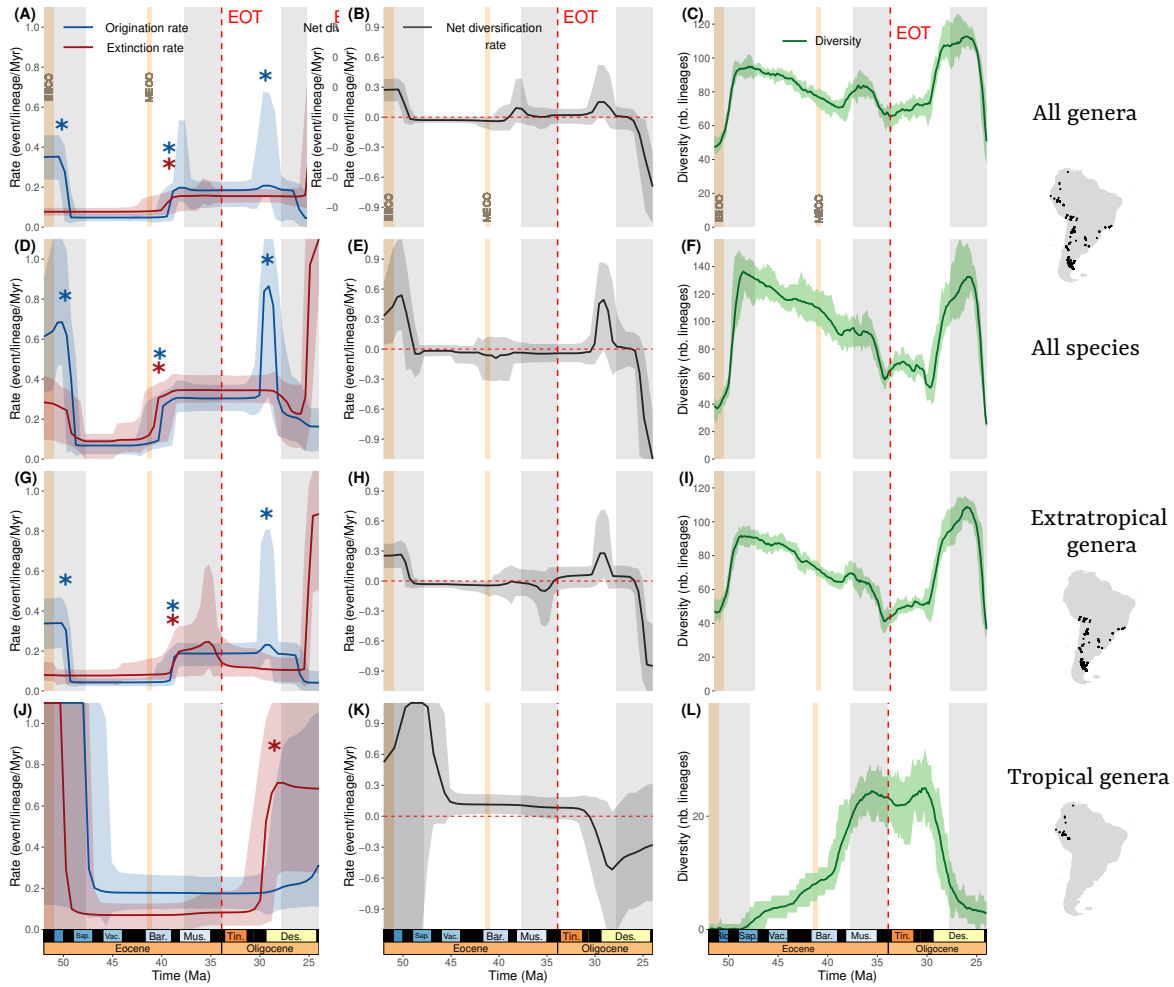

Supp. Figure 11: Diversification (estimated with RJMCMC) and diversity dynamics of South American Mammals from the early Eocene to the Late Oligocene (without binning SALMAs to their corresponding Sub-Epochs). Trends are represented for all genera (A-C), all species (D-F), extratropical (G-I) and tropical genera (J-L). Light orange bands represent the early Eocene (53-51 Ma) and the Mid-Eocene (~41 Ma) Climate Optima, respectively abbreviated as EECO and MECO. Blue and red stars respectively represent significant shifts in origination and extinction rates.

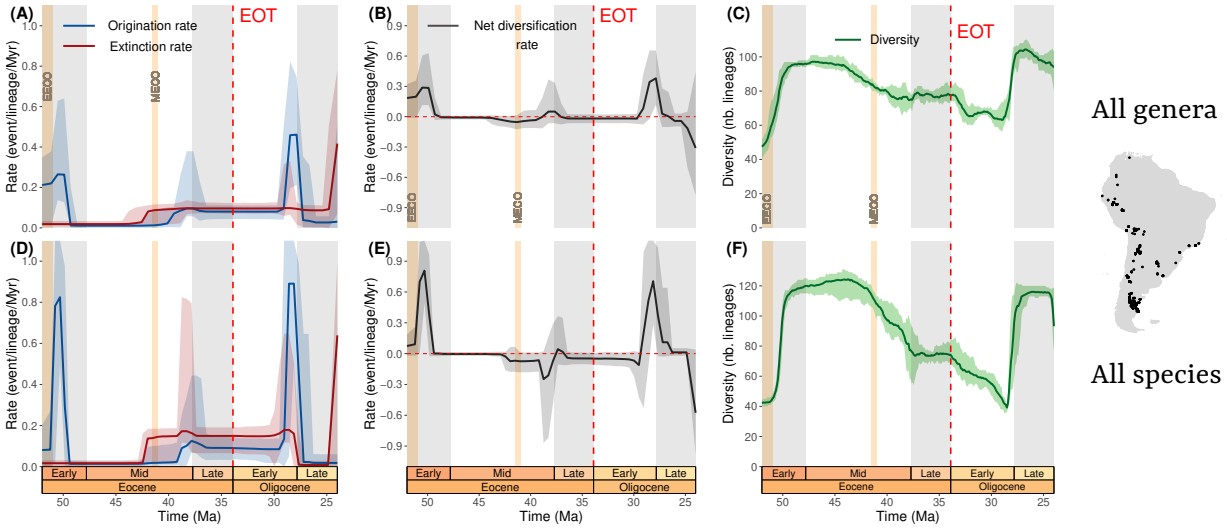

Supp. Figure 12: Diversification (estimated with RJMCMC) and diversity dynamics of South American Mammals from the early Eocene to the Late Oligocene after removing singletons (SALMA smoothed).

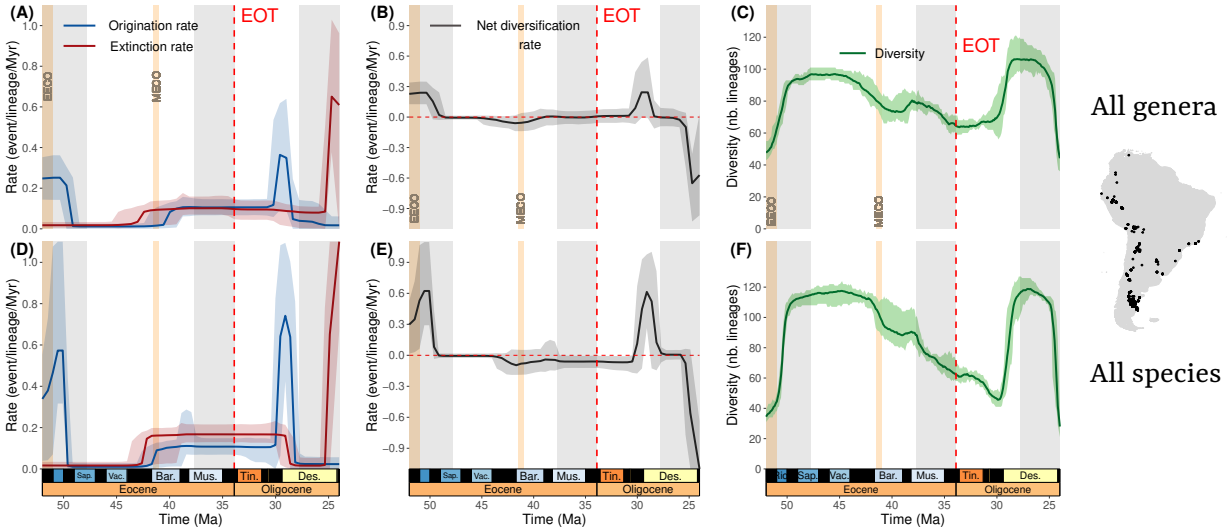

Supp. Figure 13: Diversification (estimated with RJMCMC) and diversity dynamics of South American Mammals from the early Eocene to the Late Oligocene after removing singletons (SALMA kept).

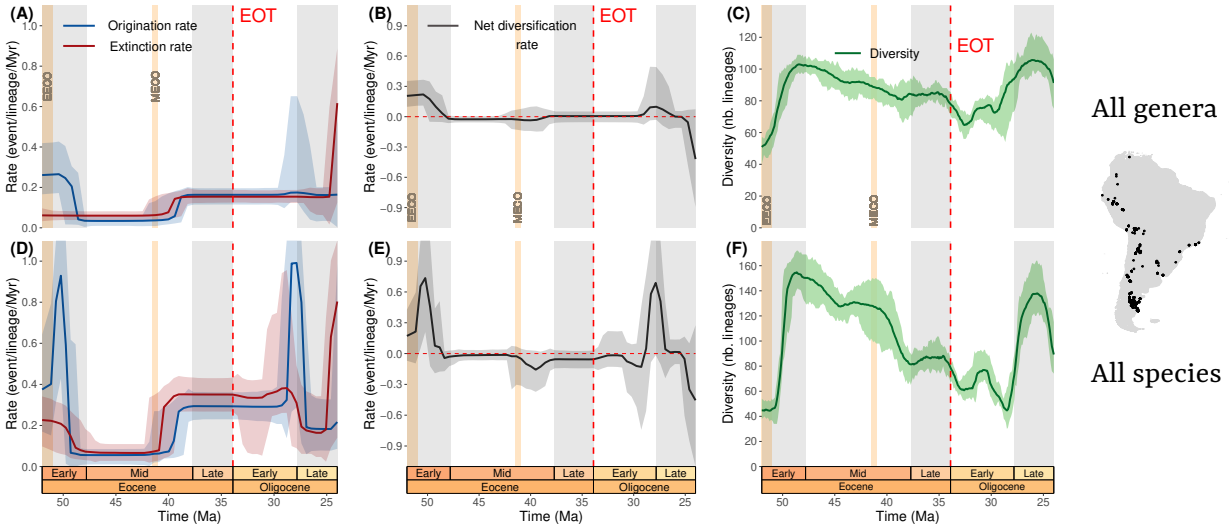

Supp. Figure 14: Diversification (estimated with RJMCMC) and diversity dynamics of South American Mammals from the early Eocene to the Late Oligocene after subsetting our dataset to unique locality-lineage combinations (SALMA smoothed).

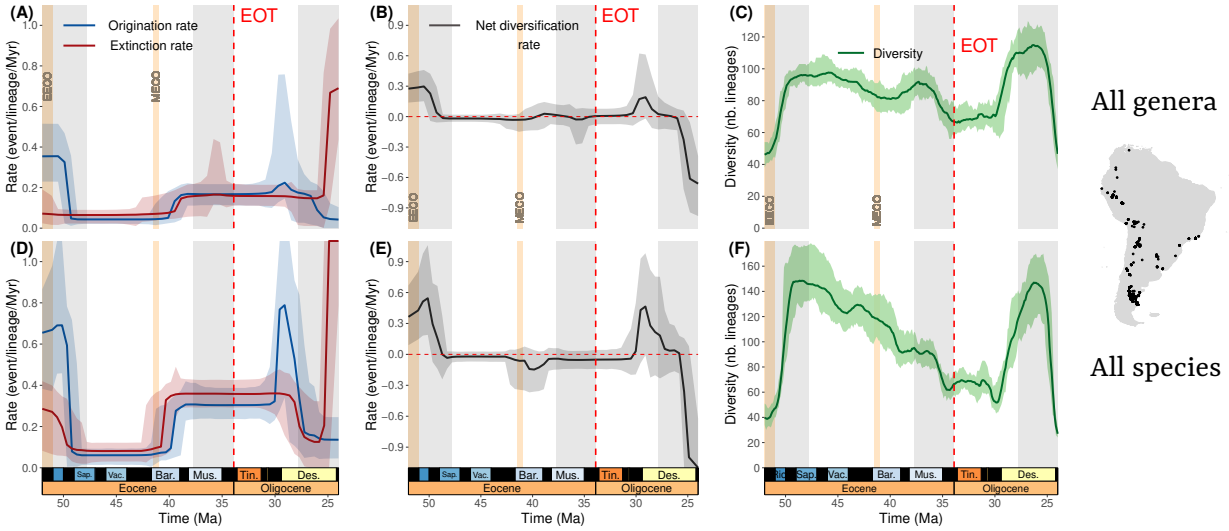

Supp. Figure 15: Diversification (estimated with RJMCMC) and diversity dynamics of South American Mammals from the early Eocene to the Late Oligocene after subsetting our dataset to unique locality-lineage combinations (SALMA kept).

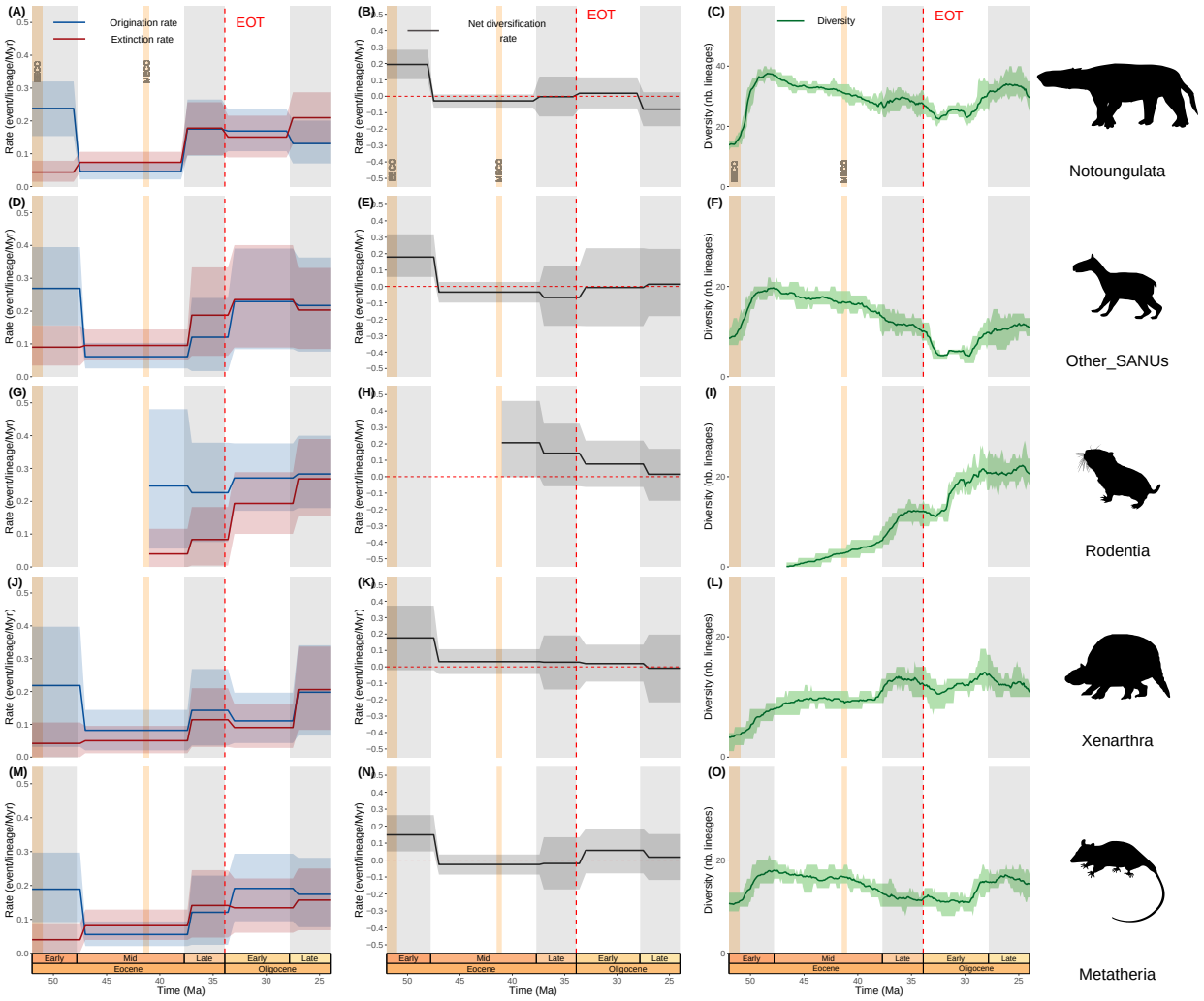

Supp. Figure 16: Genus-level diversity and diversification dynamics of five mammal groups from the early Eocene to the Late Oligocene. Diversification trends are analyzed under the BDCS algorithm using the origination and extinction times inferred by the analysis of the full dataset. Trends are represented for notoungulates (A-C), all the other native ungulates ("Other_SANUs", *i.e.*, Litopterna, Astrapotheria, Pyrotheria, Xenungulata) (D-F), rodents (G-I), xenarthrans (J-L) and metatherians (M-O). Light orange bands represent the early Eocene (53-51 Ma) and the Mid-Eocene (~41 Ma) Climate Optima, respectively abbreviated EECO and MECO.

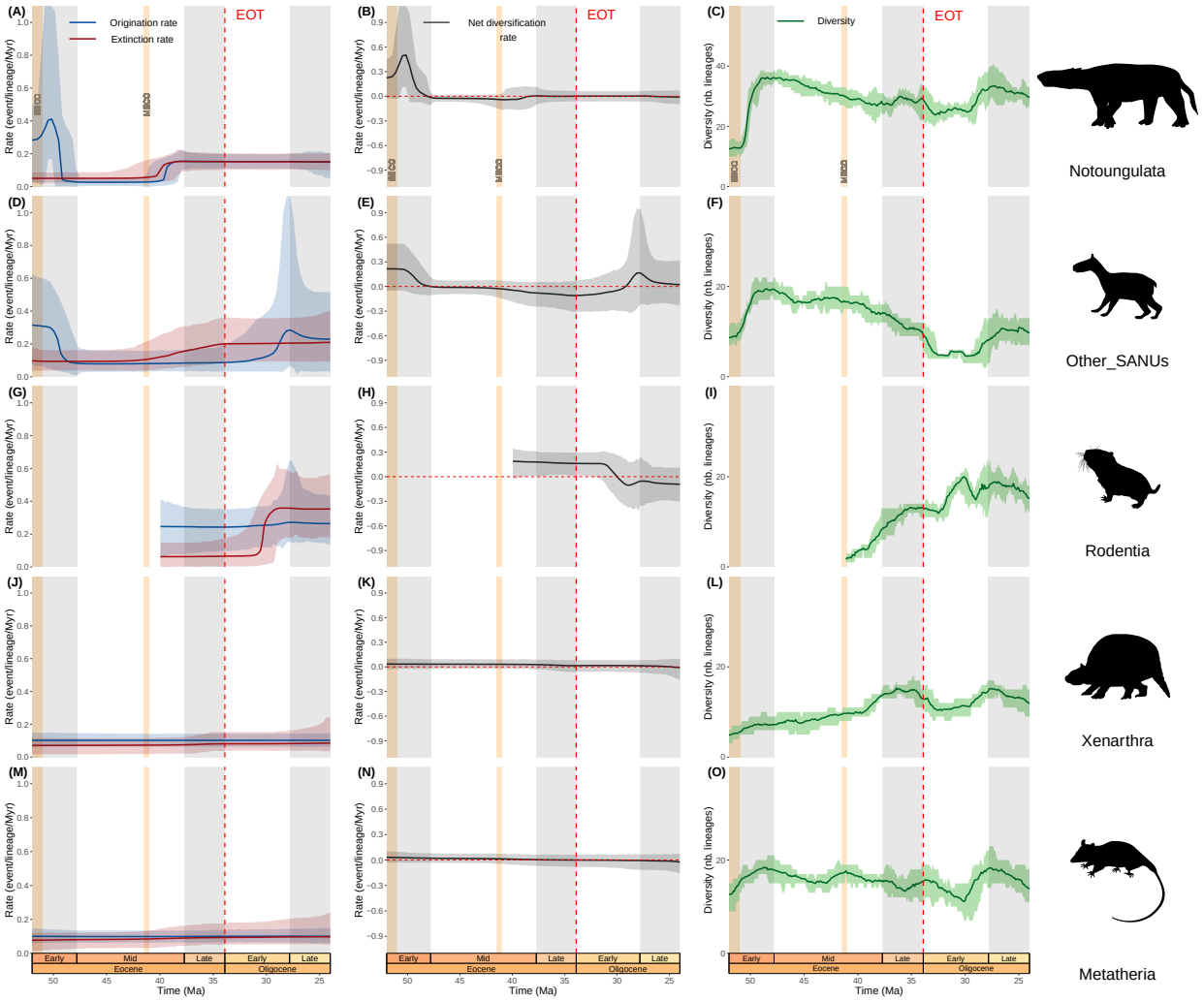

Supp. Figure 17: Genus-level diversity and diversification dynamics (inferred with RJMCMC) of five mammal groups from the early Eocene to the Late Oligocene. Diversification trends are analyzed under the RJMCMC algorithm (de-novo estimation of origination and extinction times). Trends are represented for notoungulates (A-C), all the other native ungulates ("Other_SANUs", *i.e.*, Litopterna, Astrapotheria, Pyrotheria, Xenungulata) (D-F), rodents (G-I), xenarthrans (J-L) and metatherians (M-O). Light orange bands represent the early Eocene (53-51 Ma) and the Mid-Eocene (~41 Ma) Climate Optima, respectively abbreviated EECO and MECO.

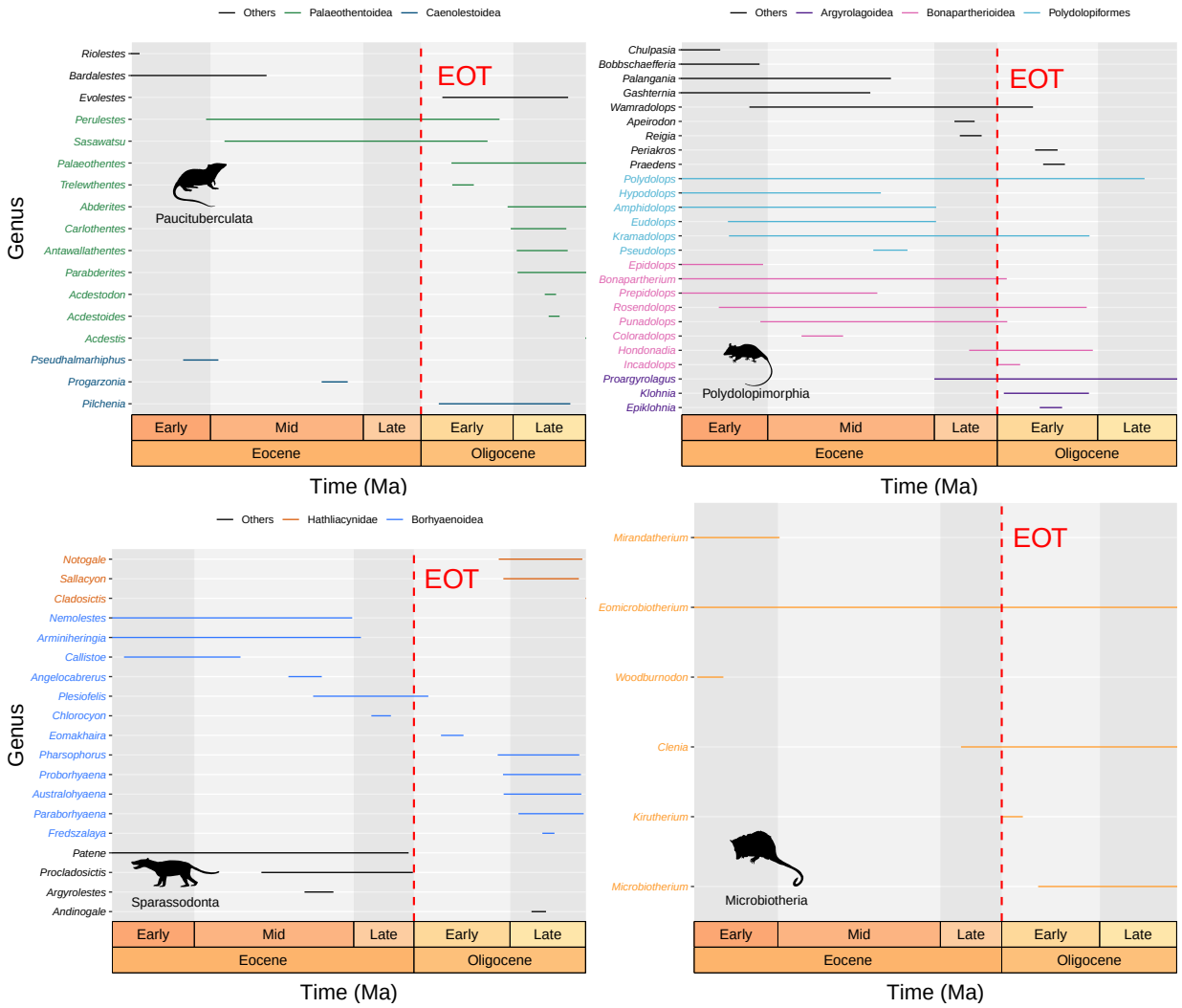

Supp. Figure 18: Metatherian genera longevity across the Eocene-Oligocene. Each panel represents a phylogenetic order, within which each genera are colored based on their superfamily. Following Antoine et al. (2021), we chose to nest the superfamily Argyrolagoidea inside Polydolopimorphia, but we know that this phylogenetic placement is under debate (see Beck (2017)).

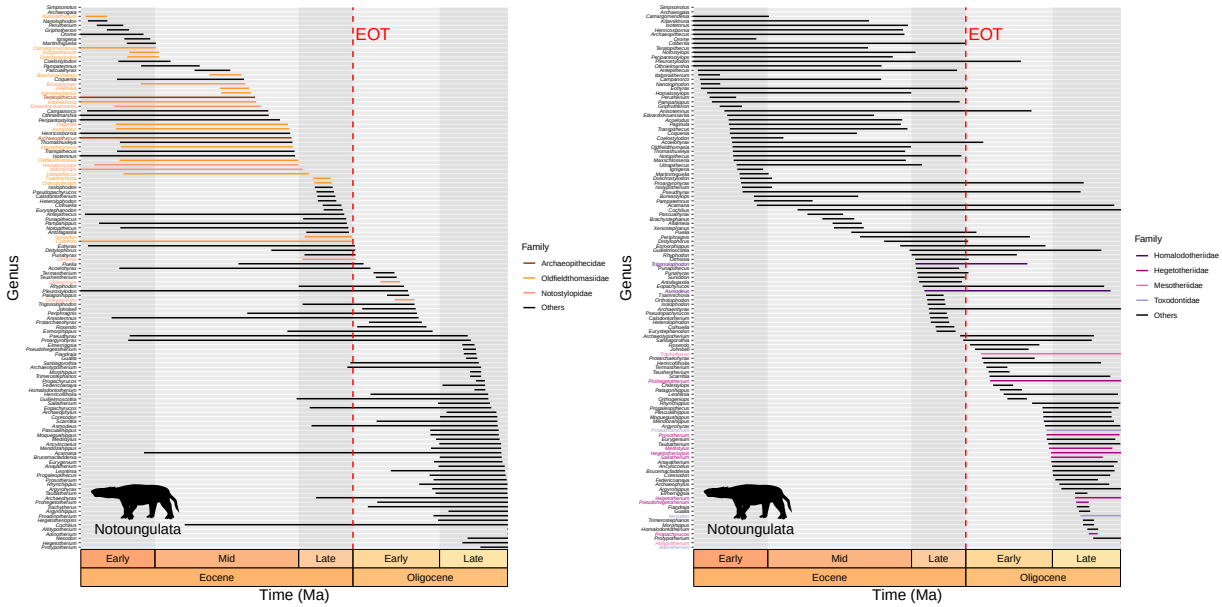

Supp. Figure 19: Notoungulate genera longevity across the Eocene-Oligocene. Both plots display the exact same information. On the left panel, genera were organised by increasing age of extinction, and we highlighted with colors members from three basal families going extinct near the EOT (Oldfieldthomasiidae, Archaeopithecidae and Notostylopidae). Conversely, on the right panel, genera were organised by increasing age of origination, and we highlighted with colors members of families originating near the EOT (Homalodotheriidae, Hegetotheriidae, Mesotheriidae, Toxodontidae).

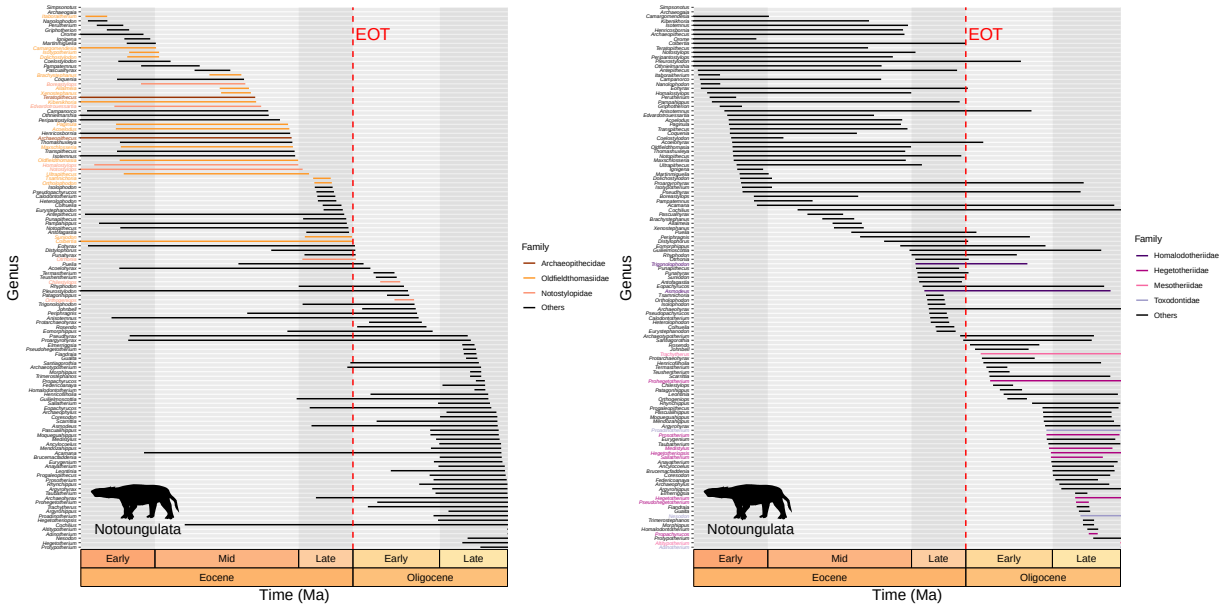

Supp. Figure 20: Notoungulate families longevity across the Eocene-Oligocene. Monophyletic families are shown in black whereas non-monophyletic families are shown in grey. Information about each family's monophyly was extracted from the phylogenetic reconstruction proposed by Billet et al. (2011).

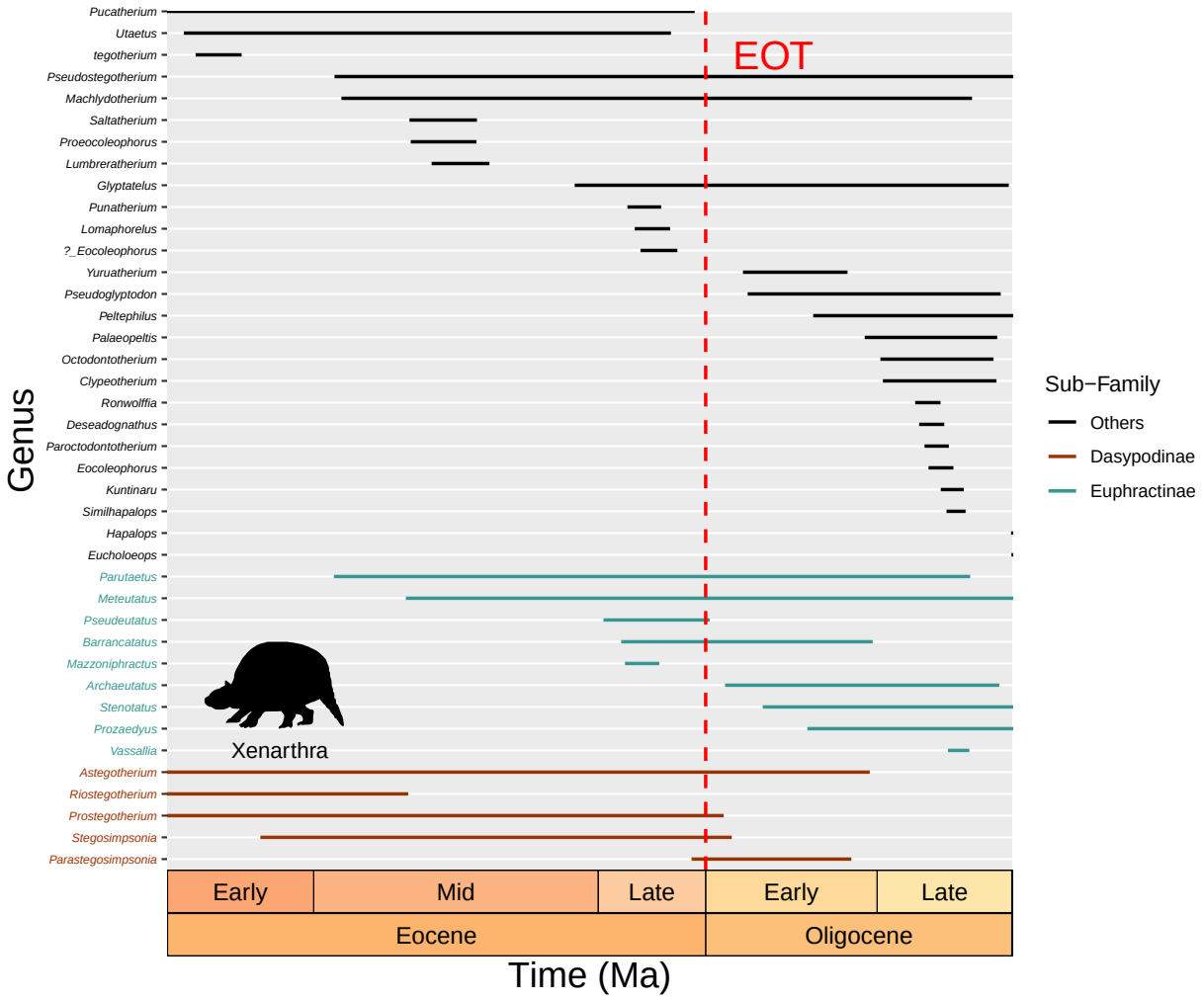

Supp. Figure 21: Xenarthran genera longevity across the Eocene-Oligocene. Genera were colored based on their affinity with two cingulate subfamilies: Dasypodinae and Euphractinae.

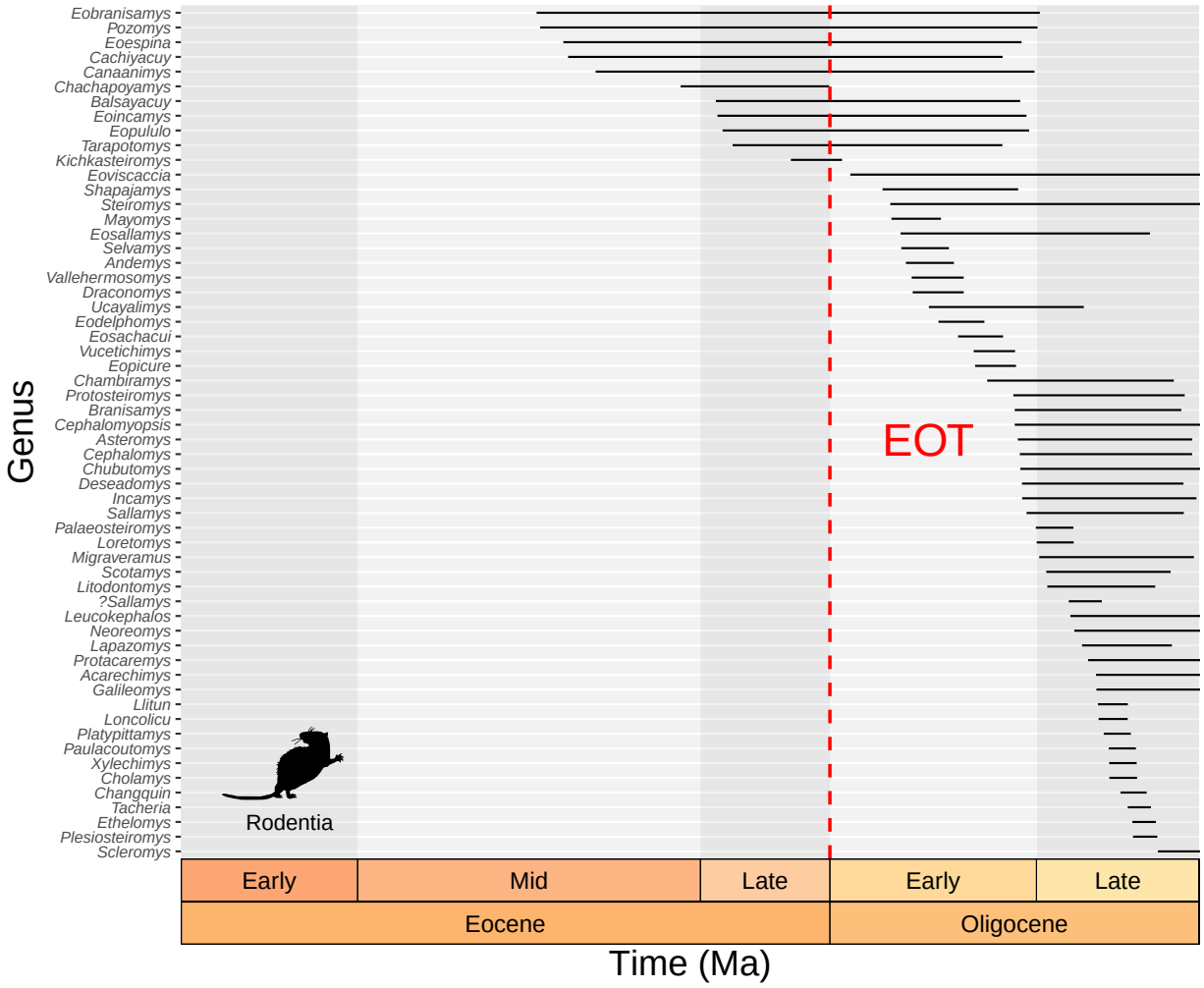

Supp. Figure 22: Rodent genera longevity across the Eocene-Oligocene interval.

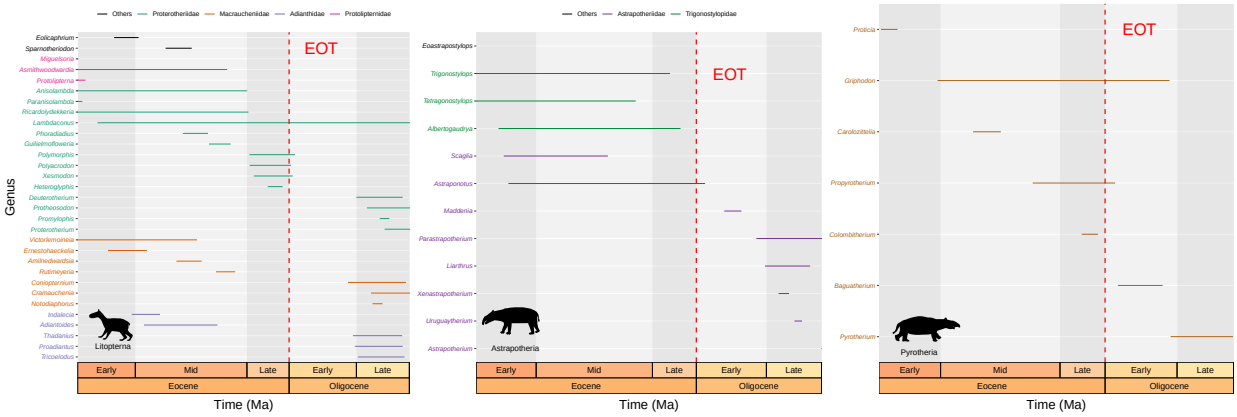

Supp. Figure 23: South American Native Ungulate genera longevity across the Eocene-Oligocene (without Notoungulata). Each panel represents a taxonomic order, within which genera are colored based on their family.

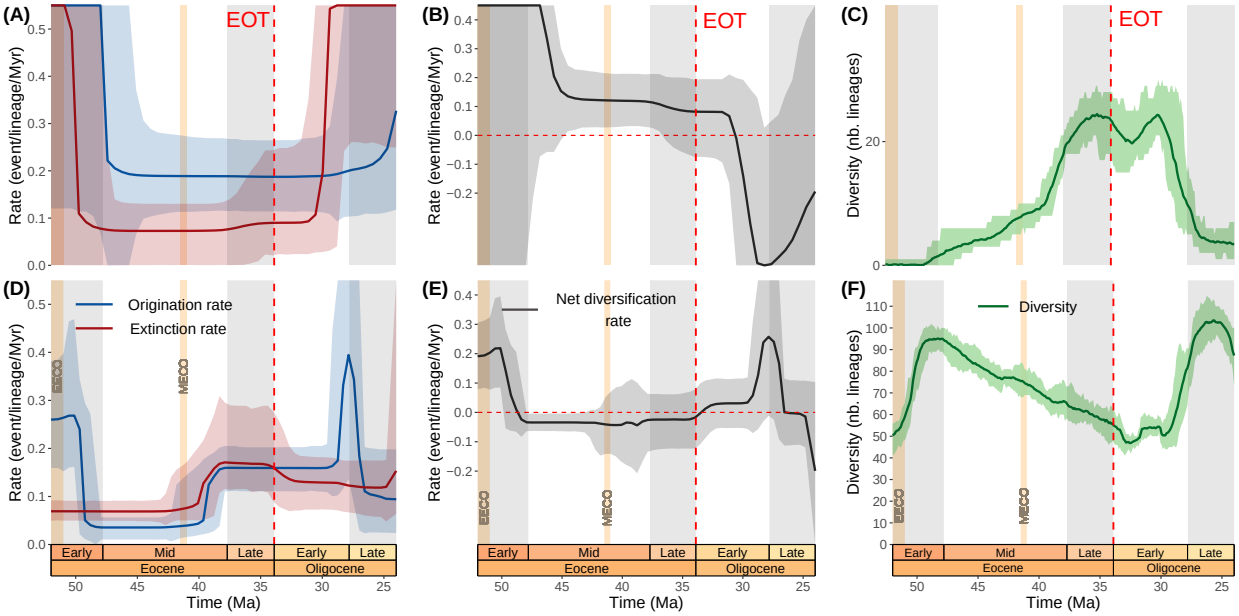

Supp. Figure 24: Diversity and diversification dynamics (inferred with RJMCMC) of South American mammal genera between the Eocene and the Oligocene arranged by latitude. Trends are assessed for the tropical (A-C) and extratropical (D-F) realms. Origination and extinction rates are respectively depicted in blue and red (A and D). Stars indicate significant rate shifts. Their net difference, being the net diversification rate, is represented in black (B and E). Diversity through time is plotted in green (C and F). The maps on the right show the localities of our extratropical (top) and tropical (bottom) occurrences. Light brown vertical bands indicate two key climate events, the early Eocene Climate Optimum (EECO, *ca.* 53–51 Ma) and the Middle Eocene Climate Optimum (MECO, *ca.* 41.5–41 Ma).

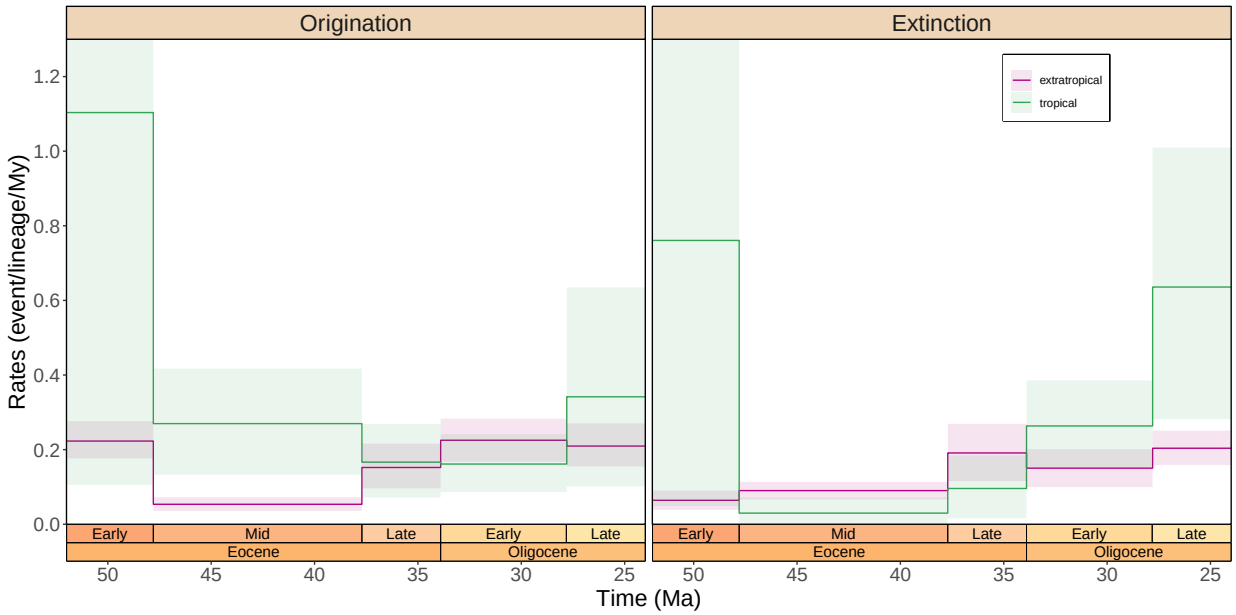

Supp. Figure 25: Tropical and extratropical origination and extinction rates inferred by the BDCS model allowing for rate shift at every geological stage (SALMA smoothed). Tropical and extratropical rates are respectively shown in green and pink, both for the origination (left) or the extinction (right) rate. SALMAs were smoothed to their corresponding sub-epoch.

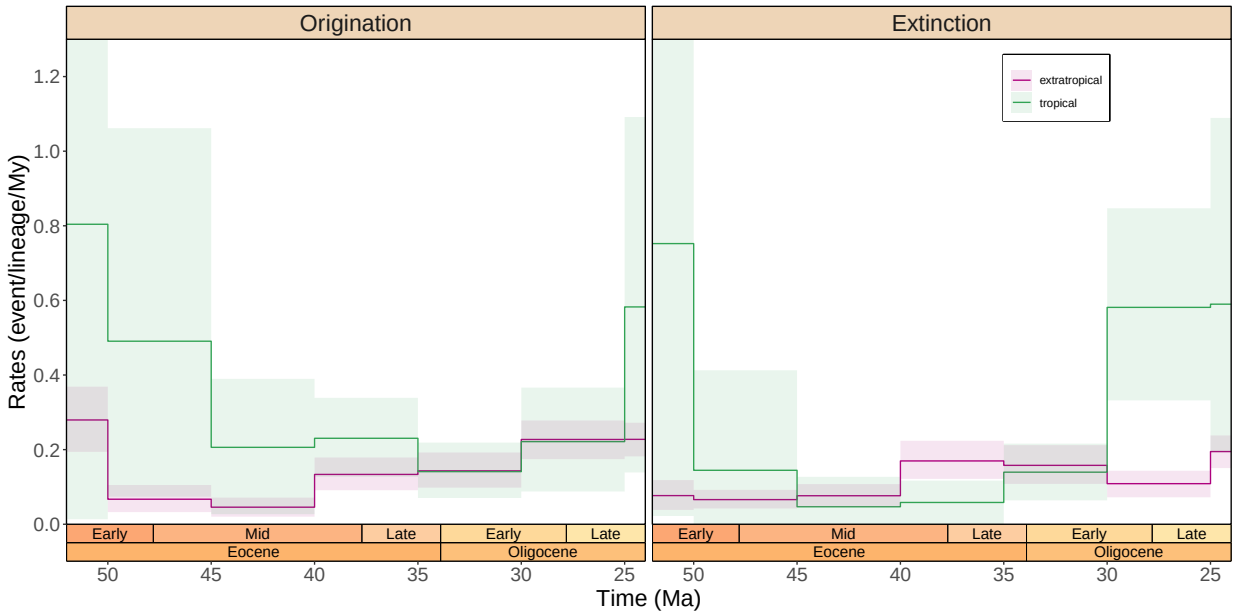

Supp. Figure 26: Tropical and extratropical origination and extinction rates inferred by the BDCS model allowing for rate shift every 5 My (SALMA smoothed). Tropical and extratropical rates are respectively shown in green and pink, both for the origination (left) or the extinction (right) rate. SALMAs were smoothed to their corresponding sub-epoch.

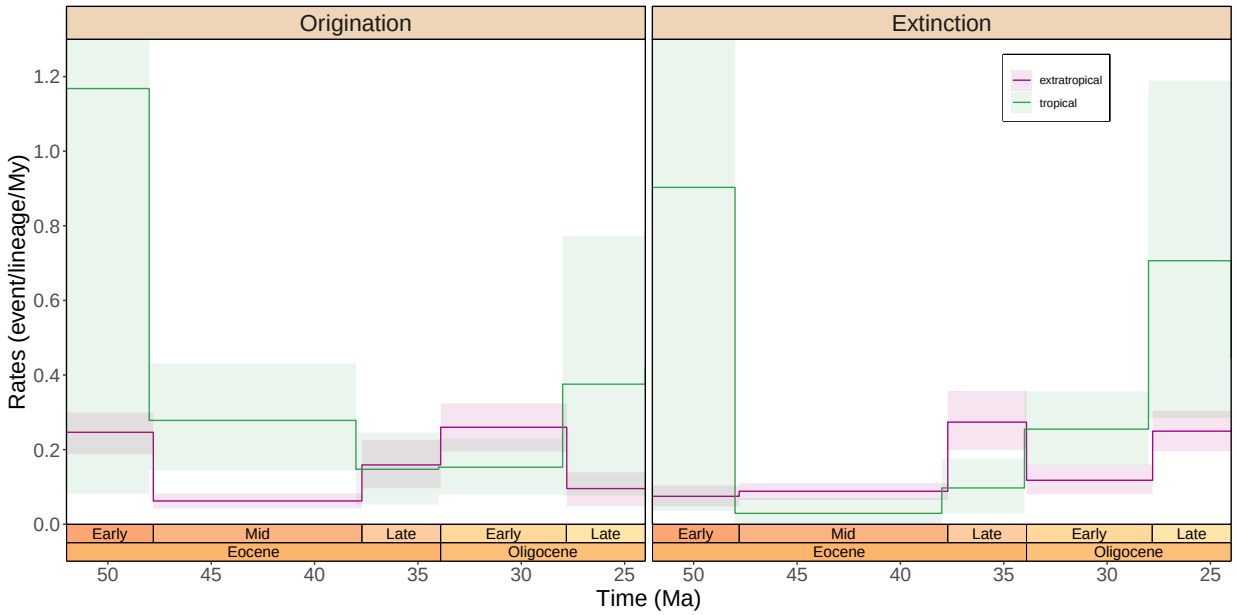

Supp. Figure 27: Tropical and extratropical origination and extinction rates inferred by the BDCS model allowing for rate shift at every geological stage (SALMA kept). Tropical and extratropical rates are respectively shown in green and pink, both for the origination (left) or the extinction (right) rate.

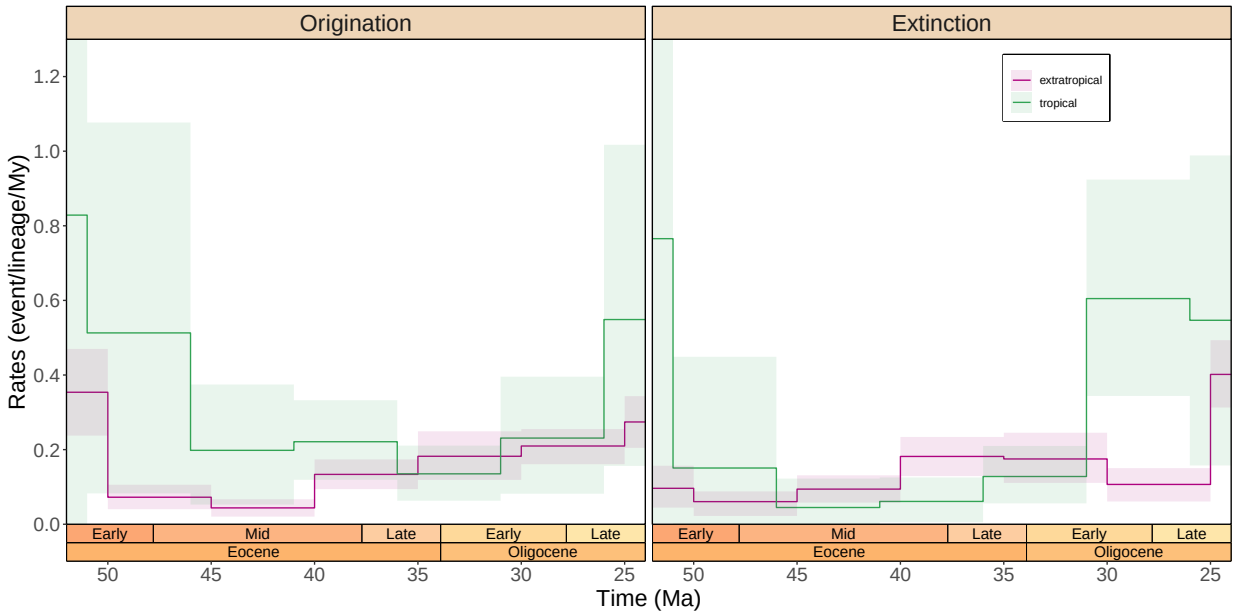

Supp. Figure 28: Tropical and extratropical origination and extinction rates inferred by the BDCS model allowing for rate shift every 5 My (SALMA kept). Tropical and extratropical rates are respectively shown in green and pink, both for the origination (left) or the extinction (right) rate.

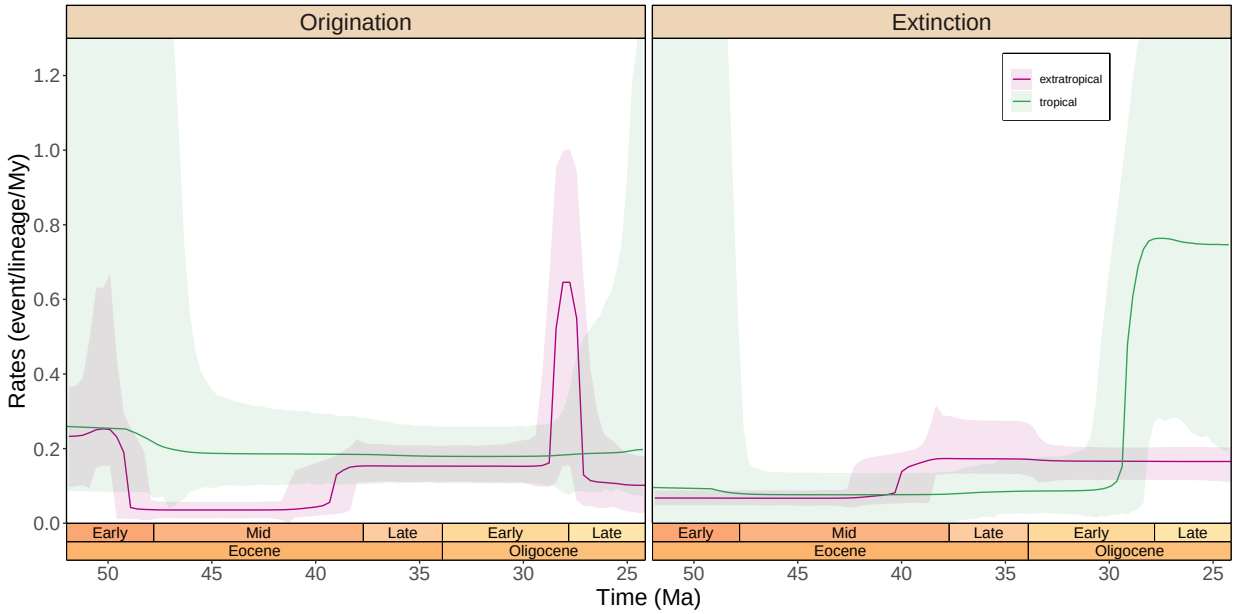

Supp. Figure 29: Tropical and extratropical origination and extinction rates inferred by the RJMCMC model allowing for rate shift every geological epoch (SALMA smoothed). Tropical and extratropical rates are respectively shown in green and pink, both for the origination (left) or the extinction (right) rate. SALMAs were smoothed to their corresponding sub-epochs.

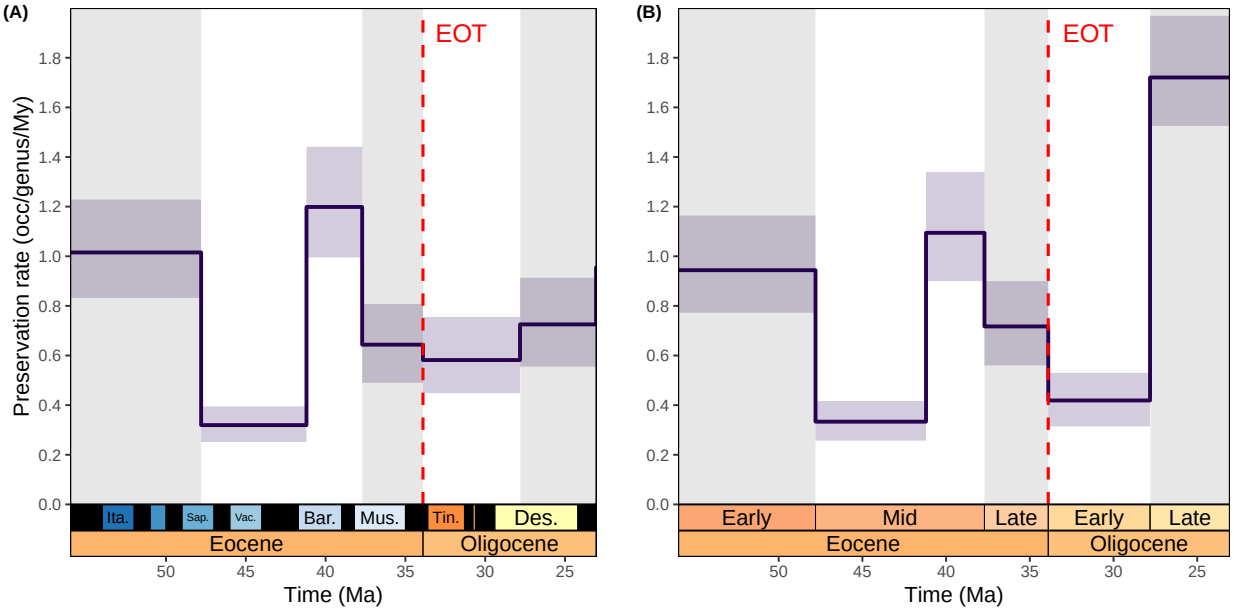

Supp. Figure 30: Estimates of the preservation rate through time in our genus-level diversification analyses. Preservation rate (*i.e.*, estimated number of preserved occurrence per genus and per million years) was estimated both in the analyses with SALMAs kept (A) and smoothed to their corresponding sub-epoch (B). Solid lines represent the mean posterior estimate, and shaded areas their 95% HPD interval. Red vertical lines show the Eocene-Oligocene Transition (EOT)

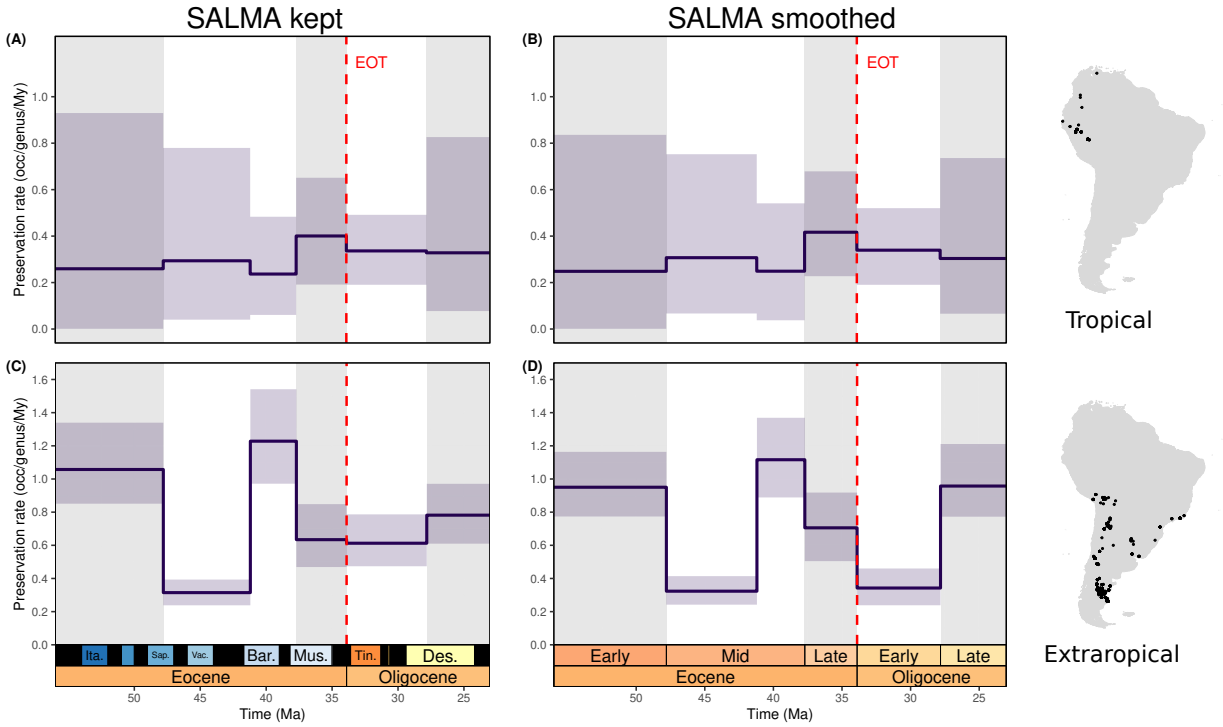

Supp. Figure 31: Estimates of the preservation rate through time and across latitude in our genus-level diversification analyses. Preservation rate (*i.e.*, estimated number of preserved occurrence per genus and per million years) was estimated for extratropical and tropical genera respectively with SALMAs kept (A and C) or smoothed to their corresponding sub-epoch (B and D). Solid lines represent the mean posterior estimate, and shaded areas their 95% HPD interval. Red vertical lines show the Eocene-Oligocene Transition (EOT).

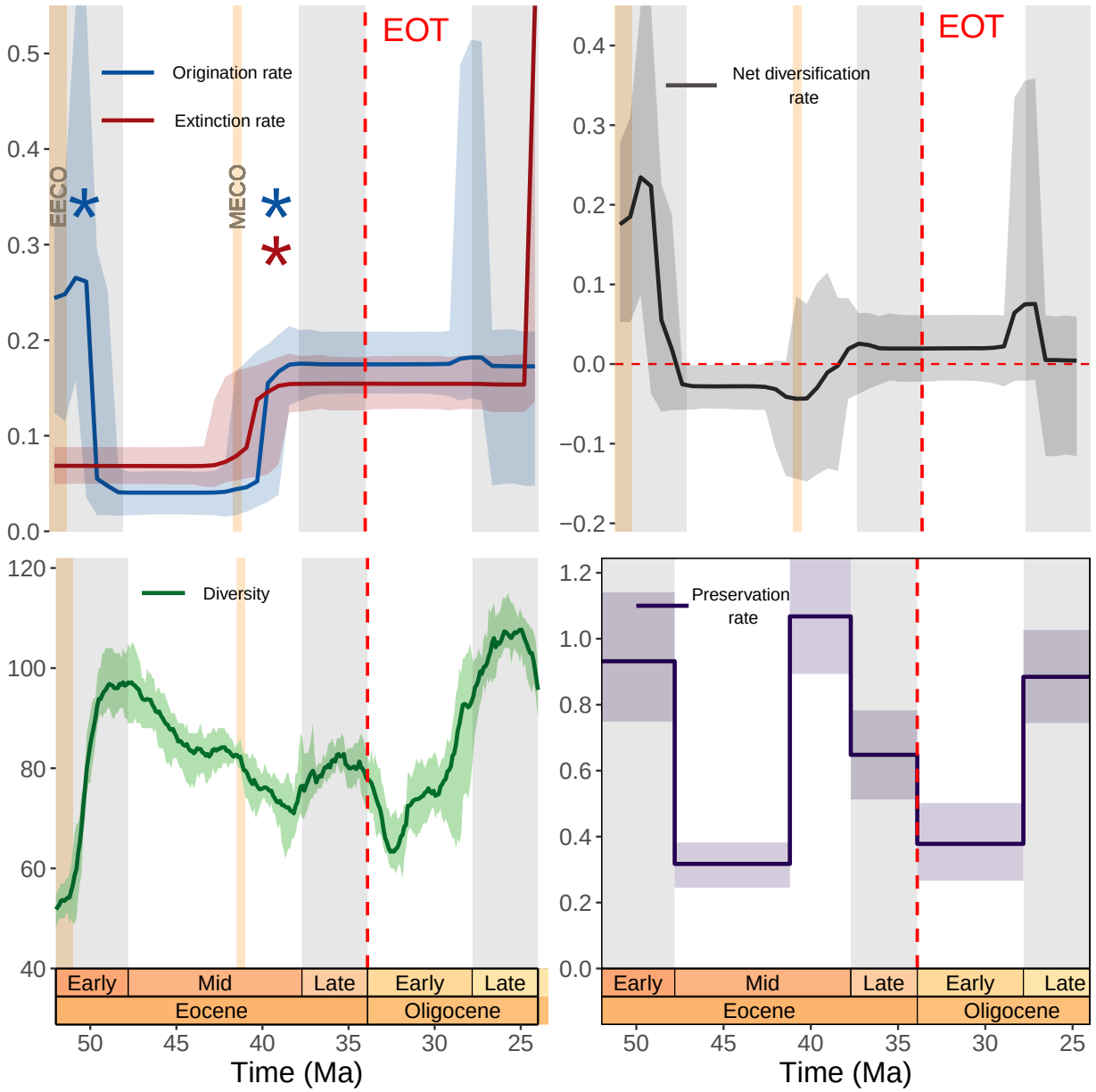

Supp. Figure 32: Diversification, diversity and preservation trends inferred from the full genus-level dataset (SALMA kept) after extending in the early Oligocene the age range western Amazonian occurrences from localities in the regions of Contamana and Tarapoto originally assigned to an Eocene age, according to Campbell et al.'s (2021) 'reverse tip-dating' inferences on concerned localities, further amalgamated as local faunas.

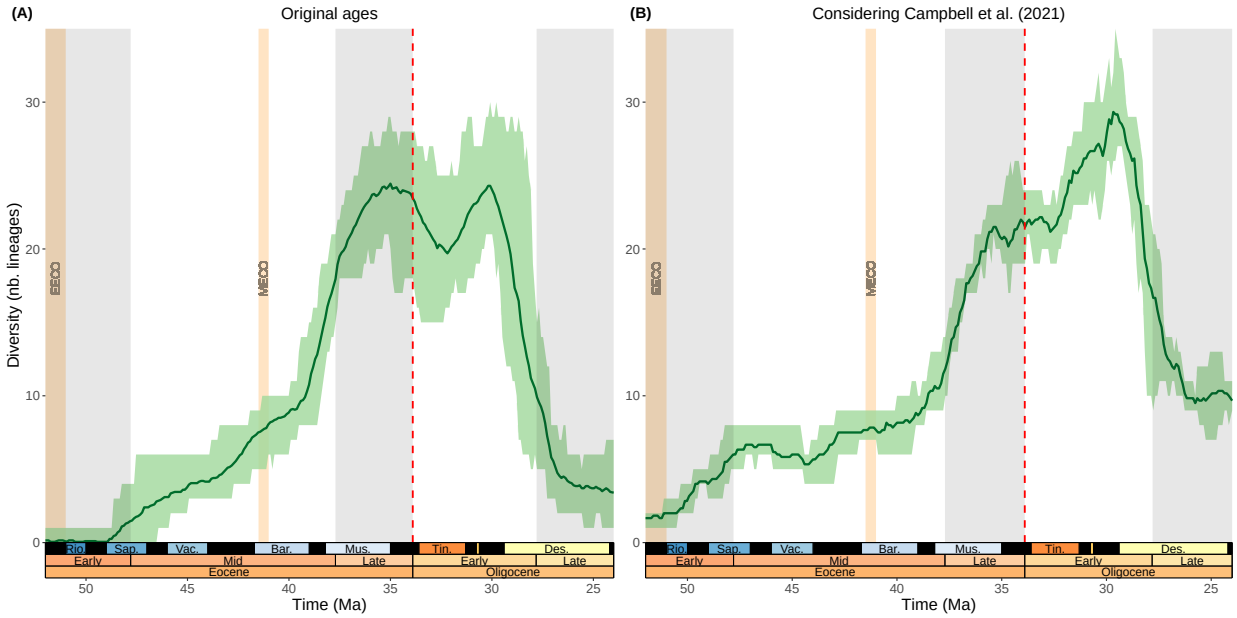

Supp. Figure 33: Diversity trends among tropical taxa obtained after extending in the early Oligocene the age range East-Amazonian occurrences from localities in the regions of Contamana and Tarapoto originally assigned to an Eocene age, according to Campbell et al.'s (2021) hypotheses (B) or not (A).

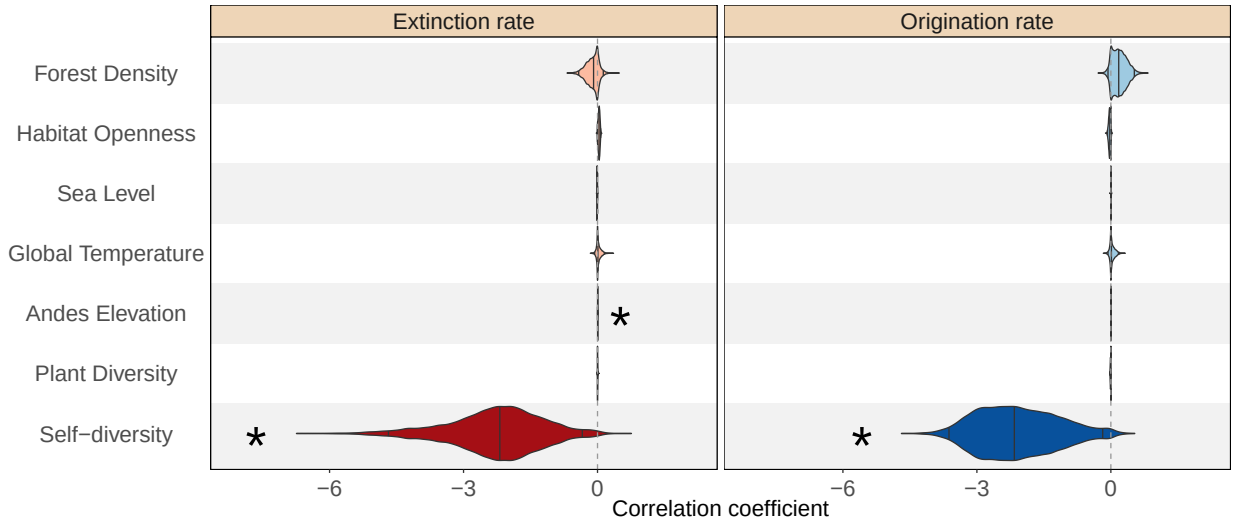

Supp. Figure 34: Bayesian estimation of correlation parameters on origination (blue) and extinction (red) rates with palaeoenvironmental covariates by considering our dataset as a whole throughout our study period. 2.5%, 50% and 97.5% quantiles are indicated in the distribution of each parameter by vertical lines, respectively from left to right. The interval between the leftmost and the rightmost vertical line of each parameter is therefore its 95% Highest Posterior Density (HPD) interval. Significant correlation coefficients, *i.e.*, having shrinkage weights > 0.5 and not including 0 in their 95% HPD are highlighted by stars and darker shades.

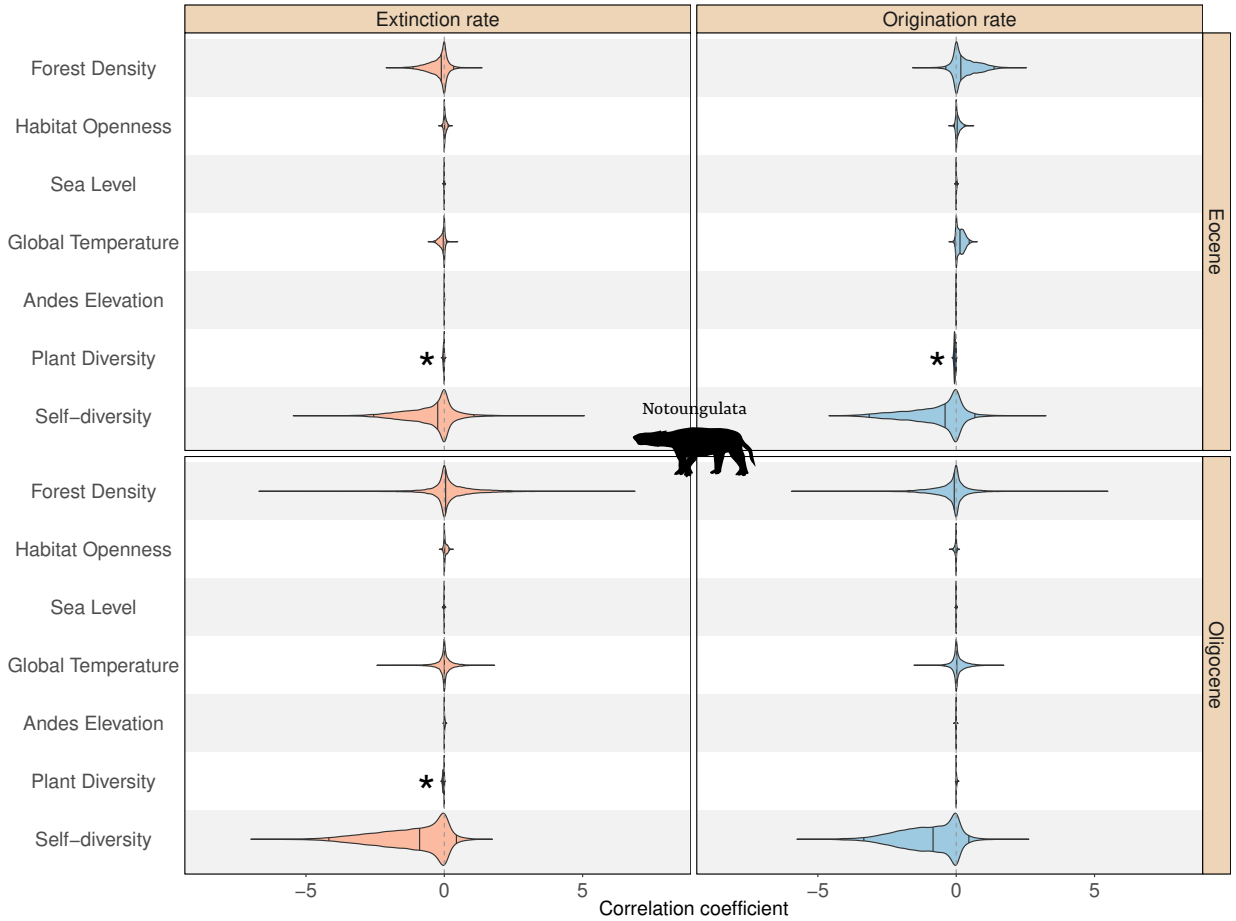

Supp. Figure 35: Bayesian estimation of correlation parameters on origination (blue) and extinction (red) rates with palaeoenvironmental covariates by constraining our analyses to notoungulate taxa. 2.5%, 50% and 97.5% quantiles are indicated in the distribution of each parameter by vertical lines, respectively from left to right. The interval between the leftmost and the rightmost vertical line of each parameter is therefore its 95% Highest Posterior Density (HPD) interval. Significant correlation coefficients, *i.e.*, having shrinkage weights > 0.5 and not including 0 in their 95% HPD are highlighted by stars and darker shades.

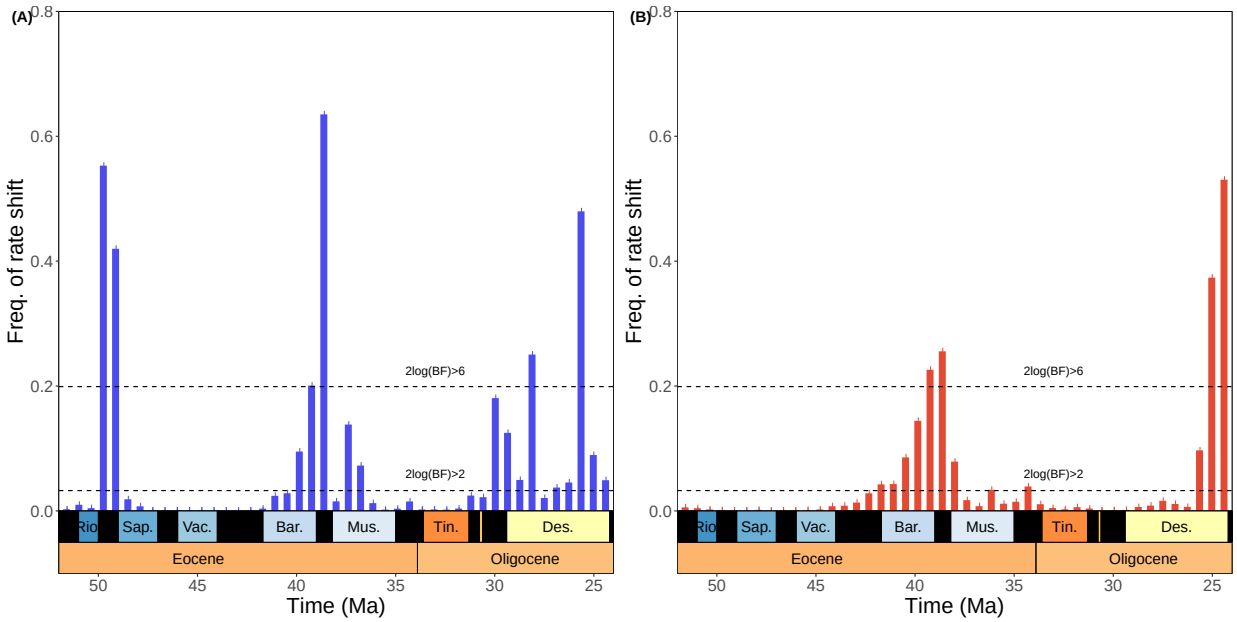

Supp. Figure 36: Frequency of extinction (A) and origination (B) rate shifts obtained from analysis of the full genus dataset with RJMCMC (SALMAs kept). Dashed horizontal lines indicate 2 * log Bayes factor of 2 and 6, respectively indicating significant and strongly-supported rate shifts

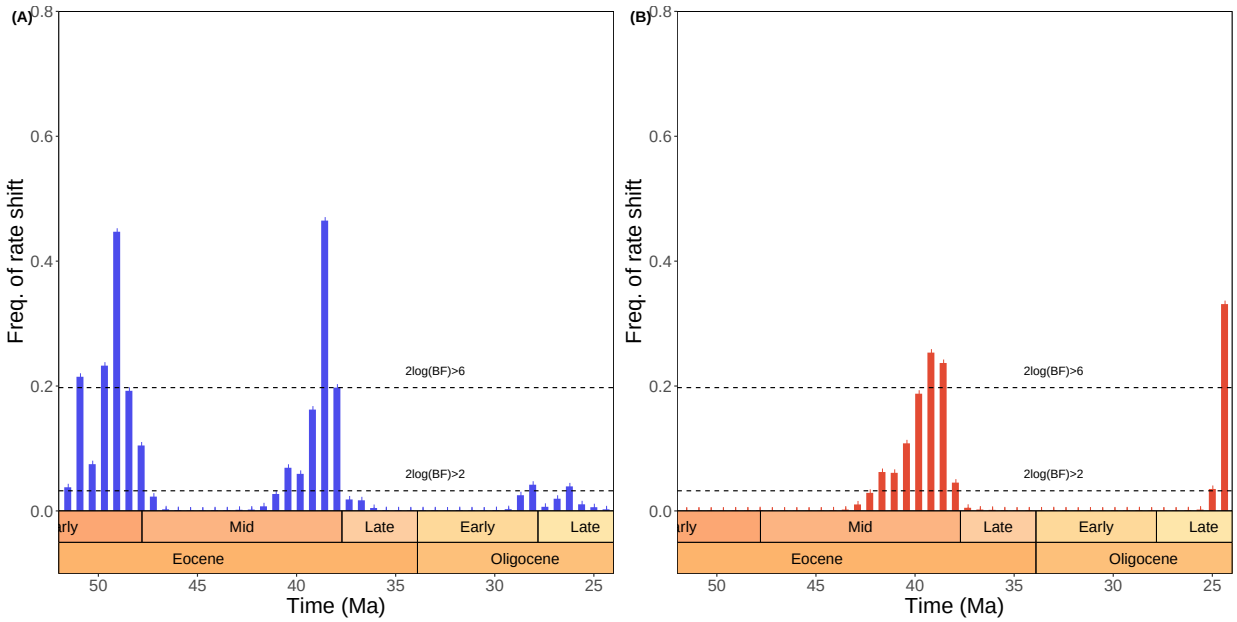

Supp. Figure 37: Frequency of extinction (A) and origination (B) rate shifts obtained from analysis of the genus dataset with RJMCMC (SALMAs smoothed). Dashed horizontal lines indicate 2 * log Bayes factor of 2 and 6, respectively indicating significant and strongly-supported rate shifts.

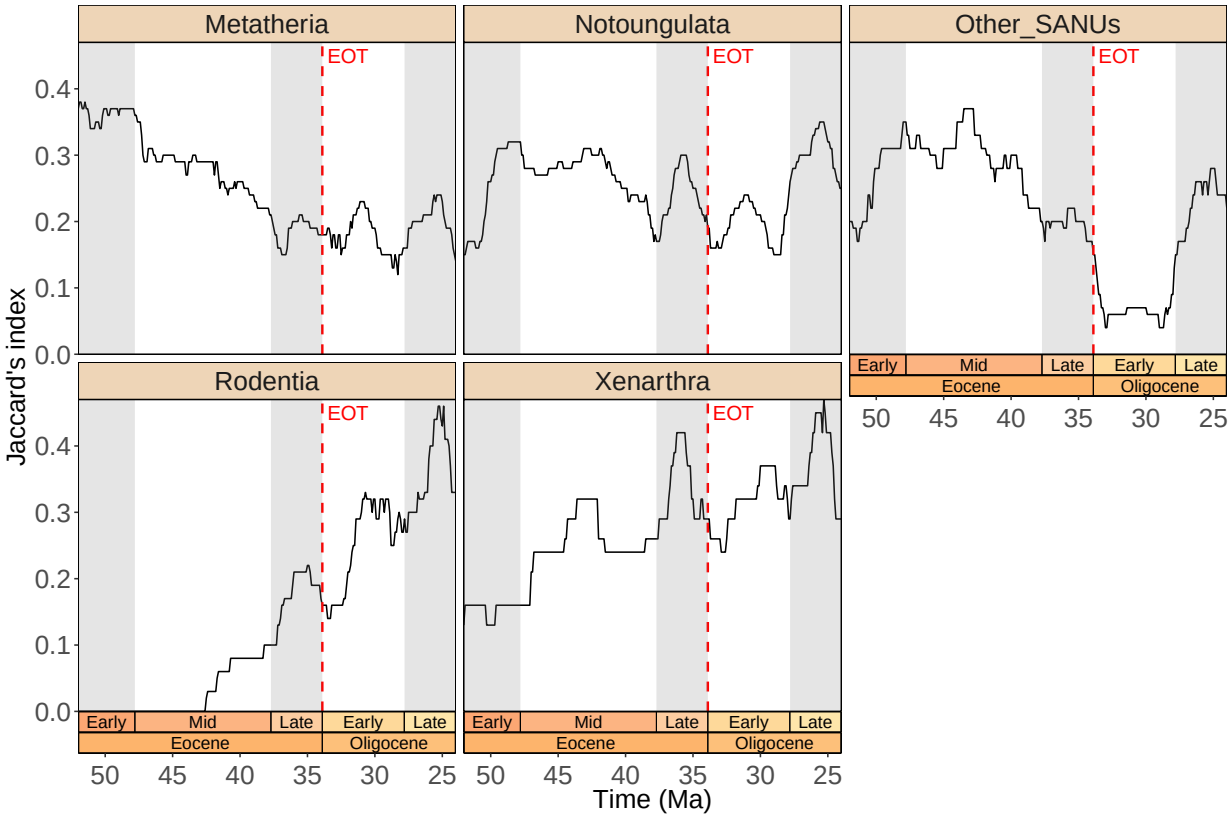

Supp. Figure 38: Taxonomic Jaccard's similarity indices through time for the five main mammal groups. Given a time t, they report how similar (in terms of shared genera) mammal assemblages were before and after t. The dashed red vertical lines indicate the EOT. Similarity values between Eocene and Oligocene faunas are always located near a local or global minimum of the similarity curve.

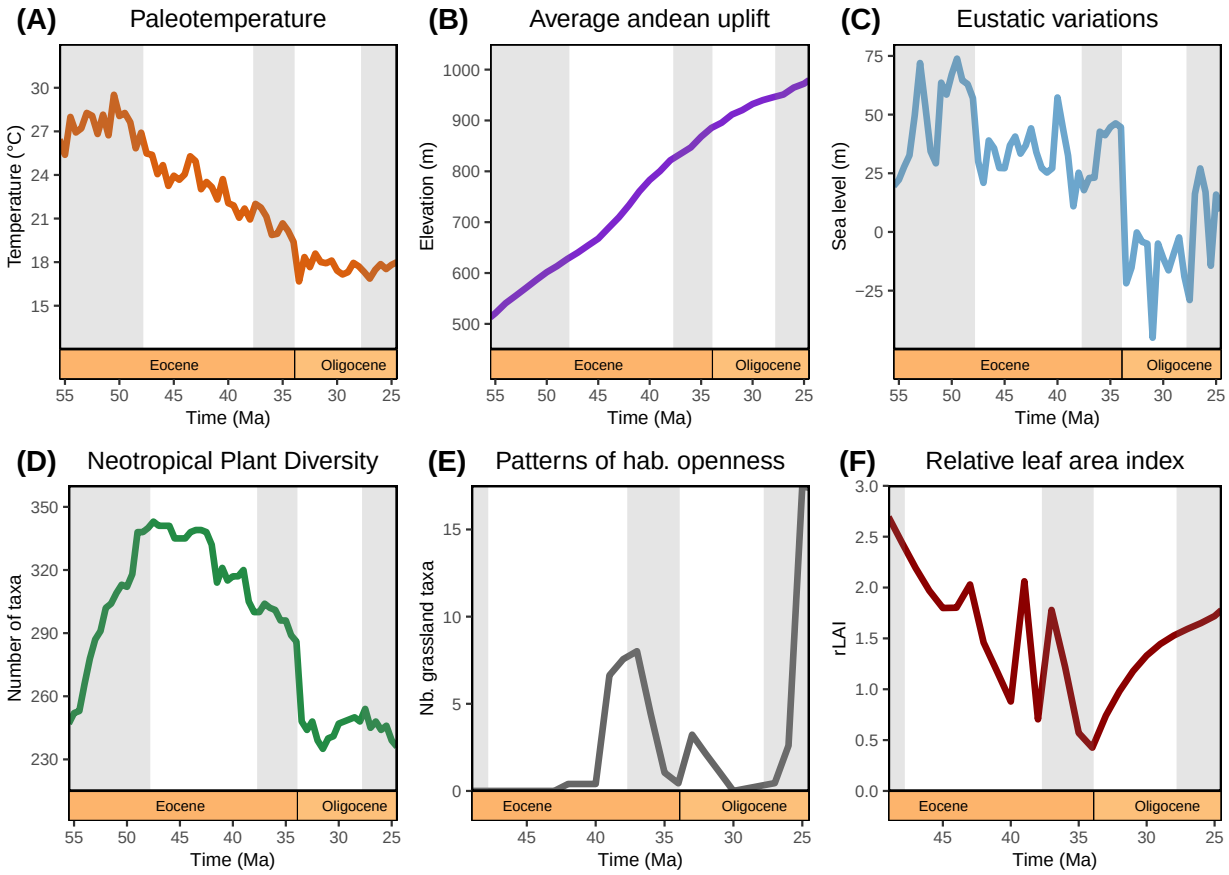

Supp. Figure 39: Environmental variables used in the Multivariate Birth-Death analyses carried out in this study. (A) Planktonic-based paleotemperature (28). (B) Andean paleoelevation (30). (C) Eustatic variations (29). (D) Neotropical plant diversity (31). (E) Temporal patterns of Patagonian open habitats (33). (F) Relative leaf area index (35). Further details on the variables are provided in **Tab. S2**.

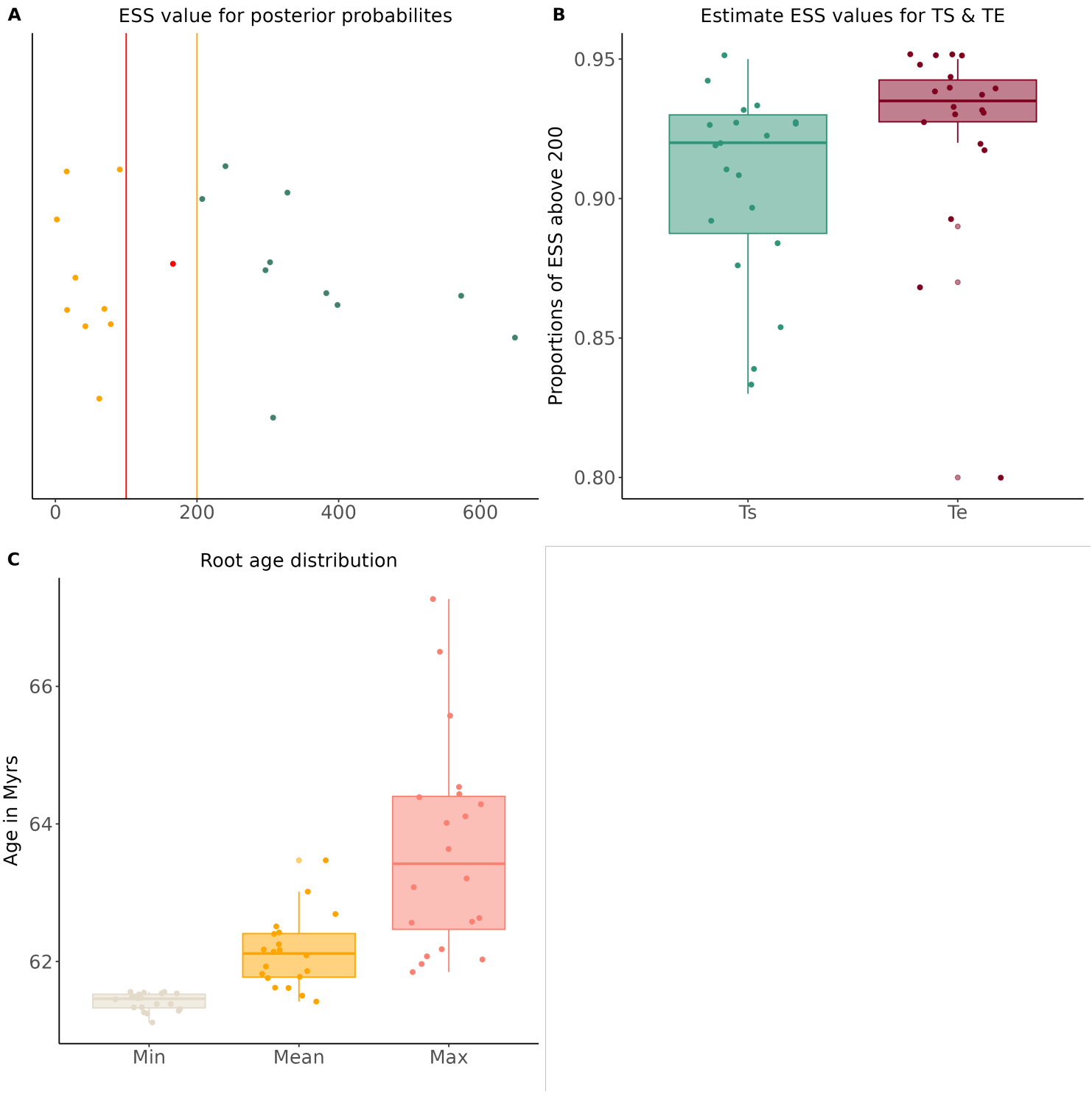

Supp. Figure 40: Convergence of our main PyRate runs.

We displayed the ESS of the model posterior probability for all the 20 replicates we ran (A). ESS greater than 200 (first-scale indicator of a run that converged, $n = 11$) are displayed in green. The proportion of origination and extinction times (resp. T_S and T_E) that converged (*i.e.*, with ESS > 200) are shown in, for each of our 20 replicates (B). The plot (C) is artefactual as it shows the posterior estimates of the mean death age of our group, together with their lower and upper boundaries of the 95% HPD interval. However, we excluded on purpose the occurrences older that 60 My.

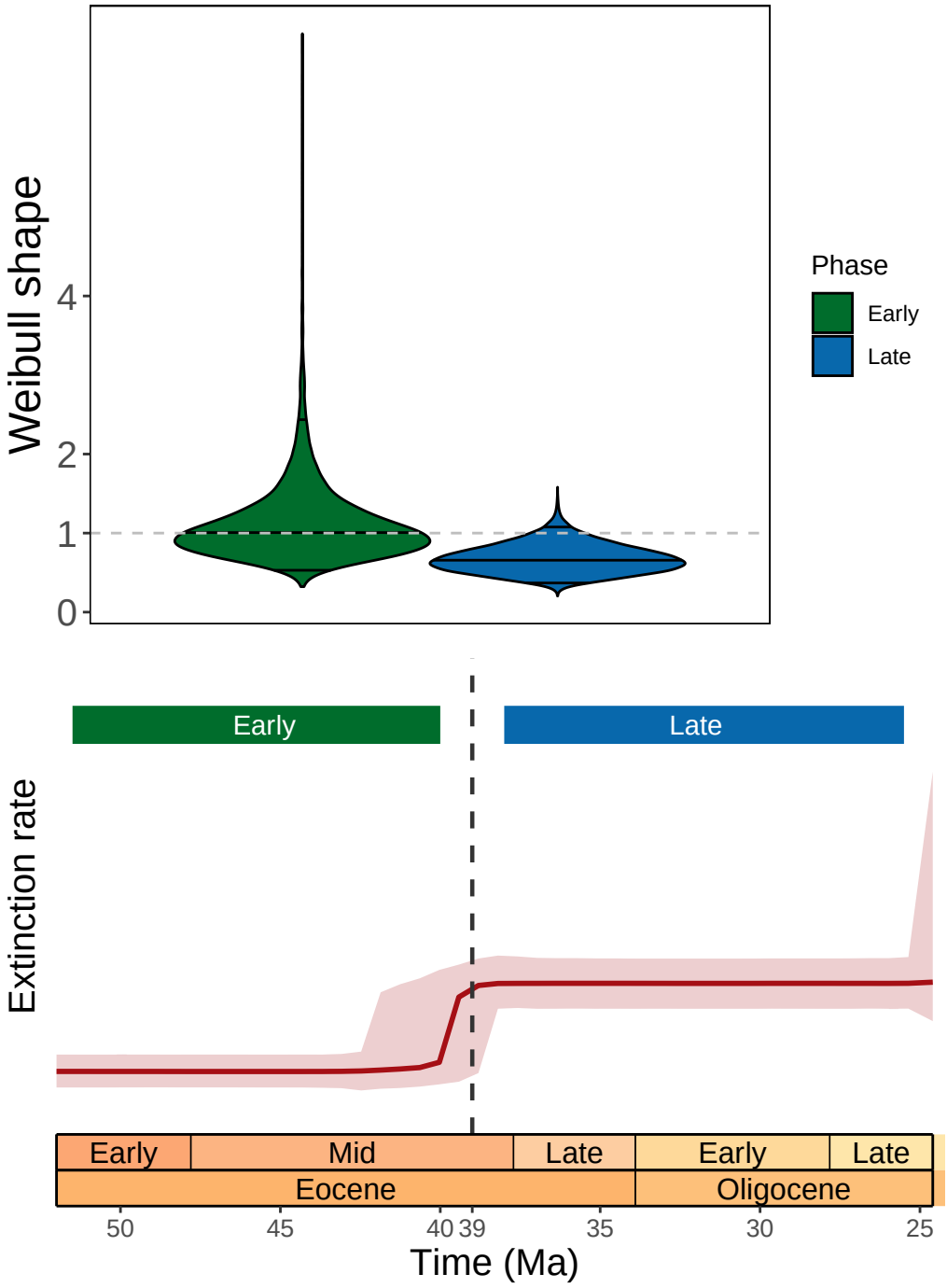

Supp. Figure 41: Posterior estimate of the shape parameter of the Weibull distribution for the ADE analyses of the 'Early' and 'Late' occurrence datasets, with constant extinction rate. 2.5%, 50% and 97.5% quantiles are indicated in the distribution of each parameter by black horizontal lines, respectively from bottom to top.

Supplementary tables

Supp. Table 1: Number of occurrences (n_occ), of genera (n_gen), of species (n_sp), of singleton (*i.e.*, genera or species only represented by a single occurrence, n_singl_gen and n_singl_sp respectively) and proportion of singletons (prop_singl_gen and prop_singl_sp) per order. The 96 occurrences (49 genera) without specified order are not displayed here, but counted in the 'Total' row.

order	n_occ	n_gen	n_singl_gen	prop_singl_gen	n_sp	n_singl_sp	prop_singl_sp
Astrapotheria	137	15	5	0.33	33	19	0.58
Stem Metatheria	46	21	9	0.43	36	28	0.78
Chiroptera	2	1	0	0	2	2	1
Cingulata	308	45	17	0.38	118	65	0.55
Dasyuromorphia	3	1	0	0	2	1	0.5
Didelphimorphia	13	5	3	0.6	7	4	0.57
Gondwanatheria	1	1	1	1	1	1	1
Groeberida	3	1	0	0	2	1	0.5
Litopterna	218	44	18	0.41	88	48	0.55
Microbiotheria	60	8	2	0.25	19	8	0.42
Notoungulata	1097	136	39	0.29	301	147	0.49
Paucituberculata	160	27	13	0.48	49	30	0.61
Pilosa	118	26	14	0.54	54	33	0.61
Polydolopimorphia	140	30	12	0.4	68	43	0.63
Primates	57	14	9	0.64	19	11	0.58
Pyrotheria	35	11	8	0.73	15	10	0.67
Rodentia	700	101	31	0.31	216	110	0.51
SANU	47	9	4	0.44	23	16	0.7
Sparassodonta	218	29	7	0.24	49	21	0.43
Xenungulata	4	2	1	0.5	4	4	1
Total	**3378**	**536**	**200**	**0.37**	**1115**	**609**	**0.55**

Supp. Table 2: Selected environmental variables chosen for the Multivariate Birth-Death analyses.

Covariate	Description	Unit	Source
Temperature	Global average temperature across the Cenozoic derived from oxygen isotopes generated using benthic Foraminifera	°C	Boshman and Condamine (2022) from Westerhold et al. (2020)
Andean uplift	Elevation data compiled from 36 geomorphological domains all across the Andes	m	Boschman (2021)
Sea level	Global eustatic variations derived from d18O and Mg/Ca records	m	Miller et al. (2020)
Neotropical plant diversity	Cenozoic (66-20 Ma) plant diversity in the Neotropics	nb. taxa	Jaramillo et al. (2006)
Habitat openness	Temporal patterns in the relative abundance of open habitats in Patagonia	nb. plant taxa	Solórzano and Nuñez (2021) from Palazzesi and Berrada (2012) and Dunn et al. (2015)
Relative Leaf Area Index (rLAI)	Quotient between leaf and ground areas, obtained via phytolith quantification on fossil leaves from Patagonia. Proxy for forest density.	m^2/m^2	Solórzano and Nuñez (2021) from Dunn et al. (2015)

Supp. Table 3: Posterior estimates of the multivariate birth-death correlation parameters with the origination rate (G_λ) for our full Eocene (52-33.9 Ma) dataset, and their associated Shrinkage weights (w_λ). Median estimates are shown along with their 95% Highest Posterior Density (HPD) interval. Significant correlations, *i.e.*, having a w_λ larger than 0.5 and of which the 95% HPD of the associated coefficients do not overlap 0 are shown in bold. In the case of temperature, the proportion of the posterior distribution of the associated G_λ below 0 is around 0.0348. Although this is larger than 0.025, we consider it small enough to claim for a significant correlation.

Covariate	G_λ	G_λ 95% HPD	$w_{G,\lambda}$	$w_{G,\lambda}$ 95% HPD
Self-diversity	**-3.24**	**[-4.749; -1.462]**	**0.892**	**[0.482; 0.996]**
Plant Diversity	-0.001	[-0.034; 0.021]	0.283	[0.001; 0.962]
Andes Elevation	0	[-0.003; 0.008]	0.251	[0; 0.962]
Global Temperature	**0.236**	**[-0.004; 0.492]**	**0.825**	**[0.025; 0.995]**
Sea Level	0.01	[-0.006; 0.041]	0.433	[0.001; 0.977]
Habitat Openness	0.087	[-0.029; 0.264]	0.429	[0.001; 0.972]
Forest Density	0.017	[-0.552; 0.69]	0.221	[0; 0.954]

Supp. Table 4: Posterior estimates of the multivariate birth-death correlation parameters with the extinction rate (G_μ) for our full Eocene (52-33.9 Ma) dataset, and their associated Shrinkage weights (w_μ). Median estimates are shown along with their 95% Highest Posterior Density (HPD) interval.

Covariate	G_μ	G_μ 95% HPD	$w_{G,\mu}$	$w_{G,\mu}$ 95% HPD
Self-diversity	-0.685	[-2.655; 0.568]	0.463	[0.002; 0.981]
Plant Diversity	-0.008	[-0.039; 0.011]	0.359	[0.001; 0.97]
Andes Elevation	0.002	[-0.001; 0.007]	0.417	[0.002; 0.974]
Global Temperature	-0.055	[-0.262; 0.059]	0.421	[0.001; 0.977]
Sea Level	-0.003	[-0.025; 0.011]	0.231	[0; 0.948]
Habitat Openness	0.001	[-0.081; 0.072]	0.109	[0; 0.924]
Forest Density	-0.024	[-0.511; 0.373]	0.186	[0; 0.947]

Supp. Table 5: Posterior estimates of the multivariate birth-death correlation parameters with the origination rate (G_λ) for our full Oligocene (33.9-23.03 Ma) dataset, and their associated Shrinkage weights (G_μ). Median estimates are shown along with their 95% Highest Posterior Density (HPD) interval.

Covariate	G_λ	G_λ 95% HPD	$w_{G,\lambda}$	$w_{G,\lambda}$ 95% HPD
Self-diversity	-0.872	[-2.399; 0.204]	0.484	[0.002; 0.973]
Plant Diversity	0.010	[-0.003; 0.036]	0.505	[0.002; 0.981]
Andes Elevation	-0.002	[-0.022; 0.008]	0.290	[0.001; 0.969]
Global Temperature	0.020	[-0.454; 0.579]	0.232	[0.001; 0.952]
Sea Level	0.000	[-0.012; 0.008]	0.149	[0; 0.929]
Habitat Openness	-0.011	[-0.101; 0.024]	0.203	[0.001; 0.95]
Forest Density	-0.007	[-1.024; 1.179]	0.208	[0; 0.959]

Supp. Table 6: Posterior estimates of the multivariate birth-death correlation parameters with the extinction rate (G_μ) for our full Oligocene (33.9-23.03 Ma) dataset, and their associated Shrinkage weights (w_μ). Median estimates are shown along with their 95% Highest Posterior Density (HPD) interval. Significant correlations, *i.e.*, having a w_μ larger than 0.5 and of which the 95% HPD of the associated coefficients do not overlap 0 are shown in bold. In the case of Andean elevation, the proportion of the posterior distribution of the associated G_μ below 0 is around 0.045. Although this is larger than 0.025, we consider it small enough to claim for a significant correlation.

Covariate	G_μ	G_μ 95% HPD	$w_{G,\mu}$	$w_{G,\mu}$ 95% HPD
Self-diversity	**-2.434**	**[-3.936; -0.811]**	**0.833**	**[0.311; 0.994]**
Plant Diversity	-0.002	[-0.047; 0.012]	0.344	[0.001; 0.981]
Andes Elevation	**0.025**	**[-0.001; 0.056]**	**0.875**	**[0.025; 0.996]**
Global Temperature	-0.009	[-0.762; 0.464]	0.2	[0; 0.959]
Sea Level	0	[-0.013; 0.016]	0.17	[0; 0.945]
Habitat Openness	-0.005	[-0.103; 0.05]	0.235	[0; 0.96]
Forest Density	0.058	[-1.328; 2.632]	0.326	[0; 0.983]

Supp. Table 7: Posterior estimates of the multivariate birth-death correlation parameters with the origination rate (G_λ) for our full dataset (56-23.03 Ma), and their associated Shrinkage weights (w_λ). Median estimates are shown along with their 95% Highest Posterior Density (HPD) interval. Significant correlations, *i.e.*, having a G_λ larger than 0.5 and of which the 95% HPD of the associated coefficients do not overlap 0 are shown in bold.

Covariate	G_μ	G_μ 95% HPD	$w_{G,\mu}$	$w_{G,\mu}$ 95% HPD
Self-diversity	**-2.434**	**[-3.936; -0.811]**	**0.833**	**[0.311; 0.994]**
Plant Diversity	-0.002	[-0.047; 0.012]	0.344	[0.001; 0.981]
Andes Elevation	**0.025**	**[-0.001; 0.056]**	**0.875**	**[0.025; 0.996]**
Global Temperature	-0.009	[-0.762; 0.464]	0.2	[0; 0.959]
Sea Level	0	[-0.013; 0.016]	0.17	[0; 0.945]
Habitat Openness	-0.005	[-0.103; 0.05]	0.235	[0; 0.96]
Forest Density	0.058	[-1.328; 2.632]	0.326	[0; 0.983]

Supp. Table 8: Posterior estimates of the multivariate birth-death correlation parameters with the origination rate (G_μ) for our full dataset (56-23.03 Ma), and their associated Shrinkage weights (w_μ). Median estimates are shown along with their 95% Highest Posterior Density (HPD) interval. Significant correlations, *i.e.*, having a G_μ larger than 0.5 and of which the 95% HPD of the associated coefficients do not overlap 0 are shown in bold.

Covariate	G_μ	G_μ 95% HPD	$w_{G,\mu}$	$w_{G,\mu}$ 95% HPD
Self-diversity	**-2.182**	**[-4.666; -0.339]**	**0.811**	**[0.155; 0.994]**
Plant Diversity	0.001	[-0.006; 0.017]	0.272	[0.001; 0.968]
Andes Elevation	0.003	[0; 0.007]	0.703	[0.059; 0.987]
Global Temperature	0.009	[-0.063; 0.155]	0.246	[0; 0.957]
Sea Level	-0.007	[-0.015; 0.001]	0.455	[0.004; 0.974]
Habitat Openness	0.035	[-0.001; 0.07]	0.382	[0.007; 0.961]
Forest Density	-0.086	[-0.42; 0.13]	0.178	[0; 0.928]

Supp. Table 9: Median estimates and associated 90 and 95% Highest Posterior Density (HPD) intervals of the Weibull shape parameters for the Age-Dependent Extinction analysis of the “early” and “late” datasets (cf. Fig. S41). We can see that one is included in the 95% HPD of both parameters. However, in the case of the “late” dataset, the upper boundary of the 95% HPD is almost equal to one, and one is not included in the 90% HPD of the parameter, meaning that at least 90% of the distribution differs from one, which we judge large enough to claim for a significant effect of genus age on its extinction probability.

Phase	Median estimate	95% HPD	90% HPD
Early	1.01049	[0.554; 2.4363]	[0.61321; 2.04203]
Late	0.65766	[0.37816; 1.07411]	[0.40979; 0.99998]

Supp. Table 10: Size of the different climate zones (‘Tropical Affinity’) and Dental Ecomorphotypes (‘Diet’) categories, expressed in number of occurrences, genera and species.

	Tropical	**Affinity**			**Diet**	
	Tropical	Extratropical	Carnivorous	Herbivorous	Omnivorous	Insectivorous
Nb. occurrences	158	3226	220	2301	573	290
Nb. genera	78	470	31	324	116	57
Nb. species	116	1005	51	698	232	127

SI References

1. J. P. Scholl, J. J. Wiens, Diversification rates and species richness across the tree of life. *Proceedings of the Royal Society B: Biological Sciences* **283**, 20161334 (2016).

2. S. D. Tarquini, S. Ladevèze, F. J. Prevosti, The multicausal twilight of south american native mammalian predators (metatheria, sparassodonta). *Sci Rep* **12**, 1224 (2022).

3. R. E. Dunn, *et al.*, A new chronology for middle eocene–early miocene south american land mammal ages. *GSA Bulletin* **125**, 539–555 (2013).

4. M. Kouvari, "Palaeoenvironmental constraints on the diversity of eutherian terrestrial mammals through the cenozoic of south america, and the emergence of the modern-day latitudinal biodiversity gradient on the continent," University College of London. (2023).

5. H. Wickham, *et al.*, Welcome to the tidyverse. *Journal of Open Source Software* **4**, 1686 (2019).

6. L. A. Jones, *et al.*, Palaeoverse: A community-driven r package to support palaeobiological analysis. *Methods in Ecology and Evolution* **14**, 2205–2215 (2023).

7. W. Gearty, Deeptime: Plotting tools for anyone working in deep time. R package version 1.0.1. (2023).

8. C. Jouault, A. Nel, F. Legendre, F. L. Condamine, Estimating the drivers of diversification of stoneflies through time and the limits of their fossil record. *Insect Systematics and Diversity* **6**, 4 (2022).

9. F. L. Condamine, J. Romieu, G. Guinot, Climate cooling and clade competition likely drove the decline of lamniform sharks. *Proceedings of the National Academy of Sciences* **116**, 20584–20590 (2019).

10. G. Guinot, F. L. Condamine, Global impact and selectivity of the cretaceous-paleogene mass extinction among sharks, skates, and rays. *Science* **379**, 802–806 (2023).

11. P. C. Fitzgerald, S. J. Carlson, Examining the latitudinal diversity gradient in paleozoic terebratulide brachiopods: Should singleton data be removed? *Paleobiology* **32**, 367–386 (2006).

12. M. Foote, Origination and extinction components of taxonomic diversity: General problems. *Paleobiology* **26**, 74–102 (2000).

13. D. Silvestro, N. Salamin, A. Antonelli, X. Meyer, Improved estimation of macroevolutionary rates from fossil data using a bayesian framework. *Paleobiology* **45**, 546–570 (2019).

14. I. Quintero, M. J. Landis, W. Jetz, H. Morlon, The build-up of the present-day tropical diversity of tetrapods. *Proceedings of the National Academy of Sciences* **120**, e2220672120 (2023).

15. A. S. Meseguer, F. L. Condamine, Ancient tropical extinctions at high latitudes contributed to the latitudinal diversity gradient. *Evolution* **74**, 1966–1987 (2020).

16. C. Scotese, N. M. Wright, PALEOMAP paleodigital elevation models (PaleoDEMs) for the phanerozoic PALEOMAP project (2018).

17. C. R. Scotese, H. Song, B. J. W. Mills, D. G. van der Meer, Phanerozoic paleotemperatures: The earth's changing climate during the last 540 million years. *Earth-Science Reviews* **215**, 103503 (2021).

18. D. Silvestro, J. Schnitzler, L. H. Liow, A. Antonelli, N. Salamin, Bayesian estimation of speciation and extinction from incomplete fossil occurrence data. *Systematic Biology* **63**, 349–367 (2014).

19. D. Silvestro, N. Salamin, J. Schnitzler, PyRate: A new program to estimate speciation and extinction rates from incomplete fossil data. *Methods in Ecology and Evolution* **5**, 1126–1131 (2014).

20. D. Silvestro, B. Cascales-Miñana, C. D. Bacon, A. Antonelli, Revisiting the origin and diversification of vascular plants through a comprehensive bayesian analysis of the fossil record. *New Phytologist* **207**, 425–436 (2015).

21. T. Wiecki, *et al.*, Pymc-devs/pymc: v5.9.2 (2023) https:/doi.org/10.5281/zenodo.4603970 (November 15, 2023).

22. O. Tange, GNU parallel 20231222 ('sundhnúkagígur') (2023).

23. R Core Team, *R: A language and environment for statistical computing* (R Foundation for Statistical Computing, 2024).

24. O. Hagen, T. Andermann, T. B. Quental, A. Antonelli, D. Silvestro, Estimating age-dependent extinction: Contrasting evidence from fossils and phylogenies. *Systematic Biology* **67**, 458–474.

25. S. Lehtonen, *et al.*, Environmentally driven extinction and opportunistic origination explain fern diversification patterns. *Sci. Rep.* **7**, 4831 (2017).

26. F. L. Condamine, J. Rolland, H. Morlon, Assessing the causes of diversification slowdowns: Temperature-dependent and diversity-dependent models receive equivalent support. *Ecology Letters* **22**, 1900–1912 (2019).

27. L. M. Boschman, F. L. Condamine, Mountain radiations are not only rapid and recent: Ancient diversification of south american frog and lizard families related to paleogene andean orogeny and cenozoic climate variations. *Global and Planetary Change* **208**, 103704 (2022).

28. T. Westerhold, *et al.*, An astronomically dated record of earth's climate and its predictability over the last 66 million years. *Science* **369**, 1383–1387 (2020).

29. K. G. Miller, *et al.*, Cenozoic sea-level and cryospheric evolution from deep-sea geochemical and continental margin records. *Science Advances* **6**, eaaz1346 (2020).

30. L. M. Boschman, Andean mountain building since the late cretaceous: A paleoelevation reconstruction. *Earth-Science Reviews* **220**, 103640 (2021).

31. C. Jaramillo, M. J. Rueda, G. Mora, Cenozoic plant diversity in the neotropics. *Science* **311**, 1893–1896 (2006).

32. A. Solorzano, A. Others, Evolutionary trends of body size and hypsodonty in notoungulates and their probable drivers. *Palaeogeography, Palaeoclimatology, Palaeoecology* **568**, 123–456 (2021).

33. C. A. E. Strömberg, R. E. Dunn, R. H. Madden, M. J. Kohn, A. A. Carlini, Decoupling the spread of grasslands from the evolution of grazer-type herbivores in south america. *Nat Commun* **4**, 1478 (2013).

34. L. Palazzesi, V. Barreda, Fossil pollen records reveal a late rise of open-habitat ecosystems in patagonia. *Nat Commun* **3**, 1294 (2012).

35. R. E. Dunn, C. A. E. Strömberg, R. H. Madden, M. J. Kohn, A. A. Carlini, Linked canopy, climate, and faunal change in the cenozoic of patagonia. *Science* **347**, 258–261 (2015).

36. F. Moharrek, *et al.*, Diversification dynamics of cheilostome bryozoans based on a bayesian analysis of the fossil record. *Palaeontology* **65**, e12586 (2022).

37. M. F. Tejedor, *et al.*, New early eocene mammalian fauna from western patagonia, argentina. *American Museum Novitates* **2009**, 1–43 (2009).

38. G. G. Simpson, The beginning of the age of mammals in south america. Part 2, systematics: Notoungulata, concluded (typotheria, hegetotheria, toxodonta, notoungulata incertae sedis), astrapotheria, trigonostylopoidea, pyrotheria, xenungulata, mammalia incertae sedis. Bulletin of the AMNH; v. 137 (1967).

39. S. Roth, Noticias preliminares sobre nuevos mamíferos fósiles del cretáceo superior y terciario inferior de la patagonia. *Revista del Museo de la Plata* **11**, 135–158 (1904).

40. C. D. Frailey, Late miocene and holocene mammals, exclusive of the notoungulata, of the rio acre region, western amazonia (1986).

41. A. M. Ribeiro, Mamíferos fósiles y biocronología en el suroeste de la amazonia, brasil. *Publicación Electrónica de la Asociación Paleontológica Argentina* **14** (2013).

42. C. Goillot, P.-O. Antoine, J. Tejada, F. Pujos, R. S. Gismondi, Middle miocene uruguaytheriinae (mammalia, astrapotheria) from peruvian amazonia and a review of the astrapotheriid fossil record in northern south america. *Geodiversitas* **33**, 331–345 (2011).

43. A. Tournouër, *Note sur la géologie et la paléontologie de la patagonie* (1903).

44. F. J. Goin, A. M. Candela, New paleogene marsupials from the amazon basin of eastern peru. *The Paleogene Mammalian Fauna of Santa Rosa, Amazonian Peru. Natural History Museum of Los Angeles County, Science Series* **40**, 15–60 (2004).

45. A. M. Candela, *et al.*, The late miocene mammals from the humahuaca basin (northwestern argentina) provide new evidence on the initial stages of the great american biotic interchange. *Papers in Palaeontology* **9**, e1527 (2023).

46. P. Teta, U. F. Pardiñas, G. D'Elía, Rediscovery of chacodelphys: A south american marsupial genus previously known from a single specimen. *Mammalian Biology* **71**, 309–314 (2006).

47. N. S. Stutz, *et al.*, Late middle miocene metatheria (mammalia: Didelphimorphia and paucituberculata) from juan guerra, san martín department, peruvian amazonia. *Journal of South American Earth Sciences* **118**, 103902 (2022).

48. L. Marivaux, *et al.*, New record of neosaimiri (cebidae, platyrrhini) from the late middle miocene of peruvian amazonia. *Journal of human evolution* **146**, 102835 (2020).

49. M. A. Reguero, A. M. Candela, Late cenozoic mammals from the northwest of argentina. *Cenozoic geology of the Central Andes of Argentina* **458**, 411–426 (2011).

50. F. J. Goin, U. F. J. Pardiñas, Revisión de las especies del género hyperdidelphys ameghino, 1904 (mammalia, marsupialia, didelphidae). *Estudios geológicos* **52** (1996).

51. J. N. Gelfo, Los didolodontidae (mammalia: Ungulatomorpha) del terciario sudamericano. Sistemática, origen y evolución. *Mastozoología Neotropical* **13**, 275–277 (2006).

52. P.-O. Antoine, *et al.*, Biotic community and landscape changes around the eocene–oligocene transition at shapaja, peruvian amazonia: Regional or global drivers? *Global and Planetary Change* **202**, 103512 (2021).

53. G. Simpson, The beginning of the age of mammals in south america. Part i introduction. Edentata, condrylarthra, liptoterna, and notioprotogonia. *Bulletin of the American Museum of Natural History* **91**, 1–232 (1948).

54. F. J. Goin, M. A. Abello, Los metatheria sudamericanos de comienzos del neógeno (mioceno temprano, edad mamífero colhuehuapense): Microbiotheria y polydolopimorphia. *Ameghiniana* **50**, 51–78 (2013).

55. D. A. Croft, A. Mariano joint author Depto. Científico de Paleontología de Vertebrados Bond (Museo de La Plata La Plata, J. John, Large archaeohyracids (typotheria, notoungulata) from central chile and patagonia: Including a revision of archaeotypotherium (2003).

56. B. J. Shockey, J. J. Flynn, Morphological diversity in the postcranial skeleton of casamayoran (? Middle to late eocene) notoungulata and foot posture in notoungulates. *American Museum Novitates* **2007**, 1–26 (2007).

57. M. A. Abello, "Sistemática y bioestratigrafía de los paucituberculata (mammalia: Marsupialia) del cenozoico de américa del sur," Universidad Nacional de La Plata. (2007).

58. B. Sigé, T. Sempere, R. F. Butler, L. G. Marshall, J.-Y. Crochet, Age and stratigraphic reassessment of the fossil-bearing laguna umayo red mudstone unit, SE peru, from regional stratigraphy, fossil record, and paleomagnetism. *Geobios* **37**, 771–794 (2004).

59. G. G. Simpson, J. L. Minoprio, B. Patterson, *The mammalian fauna of the divisadero largo formation, mendoza, argentina* (Museum of Comparative Zoology at Harvard College, 1962).

60. L. Chornogubsky, Interrelationships of polydolopidae (mammalia: Marsupialia) from south america and antarctica. *Zoological Journal of the Linnean Society* **192**, 1195–1236 (2021).

61. F. Ameghino, *Notices préliminaires sur des mammifères nouveaux des terrains crétacés de patagonie* (Impr. Coni Fréres, 1902).

62. L. G. Marshall, Systematics of the extinct south american marsupial family polydolopidae (1982).

63. L. Marivaux, *et al.*, Neotropics provide insights into the emergence of new world monkeys: New dental evidence from the late oligocene of peruvian amazonia. *Journal of Human Evolution* **97**, 159–175 (2016).

64. P.-O. Antoine, *et al.*, A 60-million-year cenozoic history of western amazonian ecosystems in contamana, eastern peru. *Gondwana Research* **31**, 30–59 (2016).

65. P.-O. Antoine, *et al.*, Middle eocene rodents from peruvian amazonia reveal the pattern and timing of caviomorph origins and biogeography. *Proceedings of the Royal Society B: Biological Sciences* **279**, 1319–1326 (2012).

66. M. Boivin, *et al.*, Late middle miocene caviomorph rodents from tarapoto, peruvian amazonia. *PLoS One* **16**, e0258455 (2021).

67. M. Arnal, M. E. Pérez, L. M. Tejada Medina, K. E. Campbell Jr, The high taxonomic diversity of the palaeogene hystricognath rodents (caviomorpha) from santa rosa (peru, south america) framed within a new geochronological context. *Historical Biology* **34**, 2350–2373 (2022).

68. M. Reguero, A. Candela, R. Alonso, Biochronology and biostratigraphy of the uquía formation (pliocene–early pleistocene, NW argentina) and its significance in the great american biotic interchange. *Journal of South American Earth Sciences* **23**, 1–16 (2007).

69. M. Boivin, *et al.*, Early oligocene caviomorph rodents from shapaja, peruvian amazonia. *Palaeontographica A* **311**, 87–156 (2018).

70. M. Arnal, A. G. Kramarz, M. G. Vucetich, C. D. Frailey, K. E. Campbell Jr, New palaeogene caviomorphs (rodentia, hystricognathi) from santa rosa, peru: Systematics, biochronology, biogeography and early evolutionary trends. *Papers in Palaeontology* **6**, 193–216 (2020).

71. A. Assemat, *et al.*, Restes inédits de rongeurs caviomorphes du paléogène de la région de juanjui (amazonie péruvienne): Systématique, implications macro-évolutives et biostratigraphiques. *Geodiversitas* **41**, 699–730 (2019).

72. M. Boivin, *et al.*, Late oligocene caviomorph rodents from contamana, peruvian amazonia. *Papers in Palaeontology* **3**, 69–109 (2017).

73. C. D. Frailey, K. E. Campbell, Paleogene rodents from amazonian peru: The santa rosa local fauna. *The Paleogene Mammalian Fauna of Santa Rosa, Amazonian Peru* **40**, 71–130 (2004).

74. R. Lavocat, RONGEURS CAVIOMORPHES DE l'OLIGOCENE DE BOLIVIE. II. RONGEURS DU BASSIN DESEADIEN DE SALLA-LURIBAY.(COLLECTION HOFFSTETTER). (1976).

75. B. Patterson, A. E. Wood, *Rodents from the deseadan oligocene of bolivia and the relationships of the caviomorpha* (Museum of Comparative Zoology, Harvard University, 1982).

76. J. Hartenberger, Nouvelles découvertes de rongeurs dans le déseadien (oligocène inférieur) de salla luribay (bolivie). (1975).

77. L. Kerber, Imigrantes em um continente perdido: O registro fossilífero de roedores caviomorpha (mammalia: Rodentia: Ctenohystrica) do cenozoico do brasil. *Terrae Didática* **13**, 185–211 (2017).

78. M. Lacerda, P. S. Romano, K. L. Bandeira, L. G. SOUZA, Georeferencing fossiliferous localities from solimões and acre basins (brazil)-what we know so far about solimões formation and future perspectives. *Anais da Academia Brasileira de Ciências* **93** (2021).

79. M. E. Pérez, *et al.*, New caviomorph rodents from the late oligocene of salla, bolivia: Taxonomic, chronological, and biogeographic implications for the deseadan faunas of south america. *Journal of Systematic Palaeontology* **17**, 821–847 (2019).

80. L. G. Marshall, *Evolution of the borhyaenidae, extinct south american predaceous marsupials* (Univ of California Press, 1978).

81. F. J. Prevosti, A. M. Forasiepi, *Evolution of south american mammalian predators during the cenozoic: Paleobiogeographic and paleoenvironmental contingencies* (Springer, 2018).